On numerical solution of 1-D poroelasticity equations in a multilayered domain

A.Naumovich, O.Iliev
Fraunhofer Institut fuer Techno- und Wirtschaftsmathematik,
Gottlieb-Daimler Str. Geb.49, 67663 Kaiserslautern, Germany
{naumovic,iliev}@itwm.fhg.de

F.Gaspar, F.Lisbona,
Dept. Applied Mathematics, University of Zaragoza
Pedro Cerbuna str. 12, 50009 Zaragoza, Spain,
{fjgaspar,lisbona}@posta.unizar.es

P.Vabishchevich,
Institute for Mathematical Modelling, Russian Academy of Science,
Miusskaya sq. 4A, 125047 Moscow, Russia,
vab@rusal.ru

October 19, 2004

Keywords: poroelasticity, multilayered material, finite volume discretization, MAC type grid

Abstract

1 Introduction

In soil mechanics assumption of only vertical subsidence is often invoked and this leads to the one-dimensional model of poroelasticity. The classical model of linear poroelasticity is obtained by Biot [1], detailed derivation

can be found e.g., in [2]. This model is applicable also to modelling certain processes in geomechanics, hydrogeology, petroleum engineering (see, e.g., [3, 8], in biomechanics (e.g., [9, 10]), in filtration (e.g., filter cake formation, see [15, 16, 17]), in paper manufacturing (e.g., [11, 12]), in printing (e.g., [13]), etc.
Finite element and finite difference methods were applied by many authors for numerical solution of the Biot system of PDEs, see e.g. [3, 4, 5] and references therein. However, as it is wellknown, the standard FEM and FDM methods are subject to numerical instabilities at the first time steps. To avoid this, discretization on staggered grid was suggested in [4, 5]. A single layer deformable porous medium was considered there.
This paper can be viewed as extension of [4, 5] to the case of multilayered deformable porous media. A finite volume discretization to the interface problem for the classical one-dimensional Biot model of consolidation process is applied here. Following assumptions are supposed to be valid: each of the porous layers is composed of incompressible solid matrix, it is homogeneous and isotropic. Furthermore, one of two following assumptions is valid: porous medium is not completely saturated and fluid is incompressible or porous medium is completely saturated and fluid is slightly compressible.

The reminder of the paper is organised as follows. Next section presents the mathematical model. Third section is devoted to the dicsretization of the continuous problem. Fourth section contains the results from the numerical experiments.

2 Mathematical model

2.1 Basic equations

Classical Biot model of consolidation process for one-dimensional case consists of two following equations for unknown fluid pressure $p(x,t)$ and displacement of the solid skeleton $u(x,t)$

$$\begin{array}{c} -\frac{\partial}{\partial x}\left((\lambda+2\mu)\frac{\partial u}{\partial x}\right)+\frac{\partial p}{\partial x}=0,\ x\in(0,l),\ t\in(0,T], \\ \frac{\partial}{\partial t}\left(n\beta p+\frac{\partial u}{\partial x}\right)-\frac{\partial}{\partial x}\left(\frac{k}{\eta}\frac{\partial p}{\partial x}\right)=q(x,t),\ x\in(0,l),\ t\in(0,T], \end{array} \tag{1}$$

where λ and μ are Lame coefficients of the solid skeleton, n is porosity, β is compressibility coefficient of the fluid, k is permeability of the porous medium, η is viscosity of the fluid, $q(x,t)$ is a source term, which is used to describe forced extraction or injection process. Boundary conditions for (1)

are following:

$$p = 0,\ (\lambda + 2\mu)\frac{\partial u}{\partial x} = -u_0,\ \text{if } x = 0, \tag{2}$$

what means that this boundary is free to drain and some stress is applied on it; another boundary condition is

$$u = 0,\ \frac{\partial p}{\partial x} = 0,\ \text{if } x = l, \tag{3}$$

what means that this boundary is rigid and impermeable.
Initial condition

$$n\beta p + \frac{\partial u}{\partial x} = 0,\ \text{for } t = 0 \tag{4}$$

means that the variation in water content is zero in the beginning of the consolidation process.

Note that in the case of classical problem formulation (1) - (4) (it describes fluid flow and skeleton deformation caused by the constant vertical load applied on the top of the column of soil, bounded with rigid and impermeable bottom and lateral walls and a top, which is free to drain), system (1) can be decoupled and then the problem can be solved separately for the fluid pressure and subsequently for solid displacements. But in general case system (1) might be supplemented with another types of boundary conditions, corresponding to different physical phenomena on the boundaries, what makes decoupling impossible and simultaneous solution must be sought both for pore pressure and displacement of the solid matrix. In this paper we deal with the coupled model, what makes our approach more general and universal for modeling of the consolidation process.

2.2 Interface Problem

Consider a multilayered porous medium, where each of the layers has different physical properties. We are interested in the coupled fluid flow in the porous medium and in deformations of the porous medium when certain stress is applied to it. In this case, in addition to the basic equations given above, we have to consider interface transmission closing conditions for (1) on the interface between different layers. In the assumption of a perfect contact and a two-layer medium, the interface conditions look as follows

$$[u] = 0,\ \left[(\lambda + 2\mu)\frac{\partial u}{\partial x}\right] = 0,\ [p] = 0,\ \left[\frac{k}{\eta}\frac{\partial p}{\partial x}\right] = 0 \ \text{ for } x = \xi,\ t \in [0, T], \tag{5}$$

where $0 \le \xi \le l$ is the position of the interface between the two layers.
The coefficients of the governing equations are discontinuous across the interface, i.e.

$$\lambda = \begin{cases} \lambda_1, & x < \xi \\ \lambda_2, & x > \xi \end{cases}$$

$$\mu = \begin{cases} \mu_1, & x < \xi \\ \mu_2, & x > \xi \end{cases}$$

$$k = \begin{cases} k_1, & x < \xi \\ k_2, & x > \xi \end{cases}$$

$$n = \begin{cases} n_1, & x < \xi \\ n_2, & x > \xi \end{cases}$$

Interface conditions (5) mean continuity of the displacements and of the stress of the solid, as well as continuity of the pressure and of the velocity of the fluid across the interface between the two layers.
Let us transform the governing equations and the interface conditions to dimensionless form. The following scales are introduced

$$x := \frac{x}{l}, \quad t := \frac{(\lambda_1 + 2\mu_1)k_1 t}{\eta l^2}, \quad p := \frac{p}{u_0}, \quad u := \frac{(\lambda_1 + 2\mu_1)u}{u_0 l},$$

$$\nu := \frac{\lambda + 2\mu}{\lambda_1 + 2\mu_1}, \quad k := \frac{k}{k_1}.$$

Further, introducing new notations: $a = n\beta(\lambda_1 + 2\mu_1)$, $f(x,t) = \frac{l^2\eta}{u_0 k_1} q(x,t)$, we obtain following dimensionless form of the problem (1) - (5)

$$\begin{aligned}
&-\tfrac{\partial}{\partial x}\left(\nu \tfrac{\partial u}{\partial x}\right) + \tfrac{\partial p}{\partial x} = 0, \ x \in (0,1), \ t \in (0,T], \\
&\tfrac{\partial}{\partial t}\left(ap + \tfrac{\partial u}{\partial x}\right) - \tfrac{\partial}{\partial x}\left(k \tfrac{\partial p}{\partial x}\right) = f(x,t), \ x \in (0,1), \ t \in (0,T], \\
&\nu \tfrac{\partial u}{\partial x} = -1, \ p = 0, \ \text{if} \ \ x = 0, \ t \in (0,T], \\
&u = 0, \ \tfrac{\partial p}{\partial x} = 0, \ \text{if} \ \ x = 1, \ t \in (0,T], \\
&ap + \tfrac{\partial u}{\partial x} = 0, \ \text{if} \ \ t = 0, \ x \in (0,1), \\
&[u] = 0, \ \left[\nu \tfrac{\partial u}{\partial x}\right] = 0, \ [p] = 0, \ \left[k \tfrac{\partial p}{\partial x}\right] = 0 \ \ \text{for} \ \ x = \xi, \ t \in (0,T].
\end{aligned} \tag{6}$$

3 MAC type grid discretization.

3.1 Grids and finite volume discretization

We define two different grids: $\overline{\omega}_p$ to discretize pressure, and $\overline{\omega}_u$ to discretize displacements

$$\begin{array}{l} \overline{\omega}_p = \{x_i \mid x_i = ih,\ i = 0, \ldots, N-1\}, \\ \overline{\omega}_u = \{x_{i-0.5} \mid x_{i-0.5} = (i-0.5)h,\ i = 1, \ldots, N\}. \end{array} \tag{7}$$

We intoduse also a standard uniform grid in time with nodes $t_j = j\tau$, $j = 0, 1..., M$ with a step size $\tau = \frac{T}{M}$. Represent now the position of the interface ξ in the form $\xi = x_{n-0.5} + \theta h$, where n is some integer and $0 \leq \theta < 1$. Following the basic principles of the finite volume method (method of balance, [6]), we write balance equations for the first equation from (6) over each volume $V_{i-0.5} = (x_{i-1}, x_i)$

$$-\int\limits_{x_{i-1}}^{x_i} \frac{\partial}{\partial x}\left(\nu \frac{\partial u}{\partial x}\right) dx + \int\limits_{x_{i-1}}^{x_i} \frac{\partial p}{\partial x} dx = 0 \tag{8}$$

and for the second equation of (6) over each volume $V_i = (x_{i-0.5}, x_{i+0.5})$

$$\int\limits_{x_{i-0.5}}^{x_{i+0.5}} \frac{\partial}{\partial t}\left(ap + \frac{\partial u}{\partial x}\right) dx - \int\limits_{x_{i-0.5}}^{x_{i+0.5}} \frac{\partial}{\partial x}\left(k \frac{\partial p}{\partial x}\right) dx = \int\limits_{x_{i-0.5}}^{x_{i+0.5}} f(x,t) dx. \tag{9}$$

Consider balance equations (8), (9) and replace integrals in these equations by the following difference expressions

$$\int\limits_{x_{i-1}}^{x_i} \frac{\partial}{\partial x}\left(\nu \frac{\partial u}{\partial x}\right) dx \approx h \left(\nu p_{\bar{x}}\right)_{x, i-0.5}, \quad \int\limits_{x_{i-1}}^{x_i} \frac{\partial p}{\partial x} dx \approx h p_{\bar{x}, i},$$

$$\int\limits_{x_{i-0.5}}^{x_{i+0.5}} \frac{\partial}{\partial t}\left(ap + \frac{\partial u}{\partial x}\right) dx \approx h \left(a_i p_i + u_{\bar{x}, i+0.5}\right)_t, \tag{10}$$

$$\int\limits_{x_{i-0.5}}^{x_{i+0.5}} \frac{\partial}{\partial x}\left(k \frac{\partial p}{\partial x}\right) dx \approx h \left(k p^{\sigma}_{\bar{x}}\right)_{x, i},$$

where

$$\nu_i = \left(\frac{1}{h} \int\limits_{x_{i-0.5}}^{x_{i+0.5}} \frac{dx}{\nu(x)} \right)^{-1}, \tag{11}$$

$$a_i = \int\limits_{x_{i-0.5}}^{x_{i+0.5}} a(x)dx, \tag{12}$$

$$k_{i-0.5} = \left(\frac{1}{h} \int\limits_{x_{i-1}}^{x_i} \frac{dx}{k(x)} \right)^{-1} \tag{13}$$

and $0 \leq \sigma \leq 1$ is some weight factor.
Note, that during approximation of integrals above we applied harmonic averaging for coefficients $\nu(x)$ and $k(x)$. Substituting approximate expressions of integrals into balance equations (8) and (9), we obtain following finite-difference scheme for problem (6):

$$\begin{aligned}
&\text{for } j = 0, \ldots, M-1 \\
&-\tfrac{\nu}{h}\hat{u}_{\bar{x},i-0.5} + \hat{p}_{\bar{x},i} = 0\ , \quad i = 2, \\
&-(\nu\hat{u}_{\bar{x}})_{x,i-0.5} + \hat{p}_{\bar{x},i} = 0\ , \quad i = 3, \ldots, N-1, \\
&(ap_i + u_{x,i+0.5})_t - (kp^{\sigma}_{\bar{x}})_{x,i} = \phi^{\sigma}_i, \quad i = 1, \ldots, N-2, \\
&(ap^i + u_{x,i+0.5})_t - \tfrac{k}{h}p^{\sigma}_{\bar{x}} = \phi^{\sigma}_i, \quad i = N-1, \\
&p_0 = 0, \quad u_N = 0. \\
&ap^0_i + u^0_{x,i+0.5} = \tfrac{1}{\nu}, \quad i = 1, \ldots, N-1, \quad j = 0,
\end{aligned} \tag{14}$$

where coefficients ν, a and k are defined by formulas (11), (12), (13) respectively, and

$$\phi_i = \frac{1}{h} \int\limits_{x_{i-0.5}}^{x_{i+0.5}} f(x,t)dx.$$

In formulas (14) we used following notations $u = u^j$, $p = p^j$, $\hat{u} = u^{j+1}$, $\hat{p} = p^{j+1}$, $p^{\sigma} = (1-\sigma)p^j + \sigma p^{j+1}$.
One can show that in the case of piecewise-constant coefficients $\nu(x)$, $k(x)$

and $a(x)$ formulas (11), (13) and (12) give us following expressions for coefficients

$$\nu_i = \begin{cases} \nu_1, & i = 1, \dots, n-1, \\ \frac{\nu_1 \nu_2}{(1-\theta)\nu_1 + \theta \nu_2}, & i = n, \\ \nu_2, & i = n+1, \dots, N, \end{cases} \tag{15}$$

$$a_i = \begin{cases} a_1, & i = 1, \dots, n-1, \\ \theta a_1 + (1-\theta) a_2, & i = n, \\ a_2, & i = n+1, \dots, N, \end{cases} \tag{16}$$

$$k_{i+0.5} = \begin{cases} k_1, & i = 1, \dots, n-2, \\ \frac{k_1 k_2}{(0.5-\theta)k_1 + (0.5+\theta)k_2}, & i = n-1, \\ k_2, & i = n, \dots, N, \end{cases} \quad \text{for } \theta \le 0.5 \tag{17}$$

and

$$k_{i+0.5} = \begin{cases} k_1, & i = 1, \dots, n-1, \\ \frac{k_1 k_2}{(1.5-\theta)k_1 + (\theta-0.5)k_2}, & i = n \\ k_2, & i = n+1, \dots, N, \end{cases} \quad \text{for } \theta > 0.5. \tag{18}$$

In the case of continuous coefficients (single layered porous media), second order convergence in operator norms is proven in [4]. Theoretical analysis of (6) in the case of discontinuous coefficients is in progress and will be reported in a forthcoming paper.

3.2 Numerical results

Two sets of numerical experiments were carried out. The first set of experiments was performed in order to study numerically the convergence rate of the scheme (14). Remind, that this scheme approximates the differential problem (6), which describes deformation and fluid flow in the column, consisting of two layers of soils with different physical properties. The top of this column is free to drain, and some load is applied on it, the bottom is impermeable and rigid. We are interested in the following physical characteristics of this process: fluid pressure, fluid velocity, displacements of the solid skeleton and stresses therein.

Example 1. For the first test we choose the following values for the coefficients: $\nu_1 = 1$, $\nu_2 = \frac{\tan(\frac{1}{12})\tan(\frac{10\pi}{3})}{8\pi} \approx 0.0058$, $k_1 = 1$, $k_2 = \frac{1}{8\pi \tan(\frac{1}{12})\tan(\frac{10\pi}{3})} \approx 0.275$, $a_1 = 0$, $a_2 = 0$ and $f(x,t) = 0$. Position of the interface between two media is given by $\xi = \frac{1}{6}$. Then exact solution of a problem like (6) (but satisfying another initial conditions) is

$$p(x,t) = \begin{cases} \cos(\frac{10\pi}{3})\sin(0.5x)e^{-0.25t}, & x \le \frac{1}{6}, \\ \\ \sin(\frac{1}{12})\cos(4\pi(1-x))e^{-0.25t}, & x > \frac{1}{6}, \end{cases}$$

$$u(x,t) = \begin{cases} -2\cos(\frac{10\pi}{3})\cos(0.5x)e^{-0.25t}, & x \le \frac{1}{6}, \\ \\ -\frac{2\cos(\frac{1}{12})}{\tan(\frac{10\pi}{3})}\sin(\frac{1}{12})\sin(4\pi(1-x))e^{-0.25t}, & x > \frac{1}{6}. \end{cases}$$

These functions satisfy boundary value problem (6), the initial conditions are calculated from the above formulae at $t = 0$. Analytical expressions for the fluid velocity and for the stress of the solid are calculated from the Darcy law $v(x,t) = -k\frac{\partial p(x,t)}{\partial x}$ and from the stress-strain relationship $s(x,t) = \nu\frac{\partial u(x,t)}{\partial x}$, respectively. The resulting formulae are:

$$v(x,t) = \begin{cases} \cos(\frac{10\pi}{3})\cos(0.5x)e^{-0.25t}, & x \le \frac{1}{6}, \\ \\ \frac{\cos(\frac{1}{12})}{8\pi\tan(\frac{10\pi}{3})}\sin(\frac{1}{12})\sin(4\pi(1-x))e^{-0.25t}, & x > \frac{1}{6}, \end{cases}$$

$$s(x,t) = \begin{cases} \cos(\frac{10\pi}{3})\sin(0.5x)e^{-0.25t}, & x \le \frac{1}{6}, \\ \\ \sin(\frac{1}{12})\cos(4\pi(1-x))e^{-0.25t}, & x > \frac{1}{6}. \end{cases}$$

In our tests we compare obtained numerical solutions to the known analytical solutions and calculate relative discrete L_2-norm and relative discrete maximum norm (C-norm) of solution errors

$$\|\epsilon_w\|_c = \frac{\max\limits_{x_i \in \omega_{\bar{w}}} |w^{ex}(x_i,t_j) - w_i^{app}|}{\max\limits_{x_i \in \omega_{\bar{w}}} |w^{ex}(x_i,t_j)|}$$

and

$$\|\epsilon_w\|_{L_2} = \frac{\sum\limits_{x_i \in \omega_{\bar{w}}} |w^{ex}(x_i,t_j) - w_i^{app}|}{\max\limits_{\omega_{\bar{w}}} |w^{ex}(x_i,t_j)|},$$

where w^{ex} and w^{app} stand for the analytical and numerical solutions respectively, and $w = \{u, p, v, s\}$. We assign $\sigma = 0.5$ to the weight parameter, what allows us to obtain second order of convergence in time.

$\triangle x$	$\triangle t$	$\|\epsilon_u\|_{L_2}$	$\|\epsilon_p\|_{L_2}$	$\|\epsilon_v\|_{l_2}$	$\|\epsilon_s\|_{L_2}$
0.1	0.1	0.222E-02	0.155E+00	0.130E+00	0.739E-01
0.025	0.025	0.508E-03	0.243E-01	0.153E-01	0.106E-01
0.00625	0.00625	0.368E-04	0.105E-02	0.789E-03	0.488E-03
0.015625	0.015625	0.222E-05	0.634E-04	0.639E-04	0.298E-04
0.000390625	0.000390625	0.137E-06	0.393E-05	0.657E-05	0.185E-05

Table 1: test 1 - convergence in L_2-norm at the time moment t=0.1

$\triangle x$	$\triangle t$	$\|\epsilon_u\|_{L_2}$	$\|\epsilon_p\|_{L_2}$	$\|\epsilon_v\|_{l_2}$	$\|\epsilon_s\|_{L_2}$
0.1	0.1	0.276E-01	0.559E-01	0.737E-01	0.273E-01
0.025	0.025	0.178E-02	0.248E-02	0.399E-02	0.156E-02
0.00625	0.00625	0.107E-03	0.157E-03	0.248E-03	0.973E-04
0.015625	0.015625	0.662E-05	0.977E-05	0.159E-04	0.607E-05
0.000390625	0.000390625	0.413E-06	0.610E-06	0.110E-05	0.379E-06

Table 2: test 1 - convergence in L_2-norm at the last time moment t=1

$\triangle x$	$\triangle t$	$\|\epsilon_u\|_c$	$\|\epsilon_p\|_c$	$\|\epsilon_v\|_c$	$\|\epsilon_s\|_c$
0.1	0.1	0.518E-02	0.226E+00	0.322E+00	0.196E+00
0.025	0.025	0.306E-02	0.304E-01	0.833E-01	0.273E-01
0.00625	0.00625	0.337E-03	0.139E-02	0.470E-02	0.114E-02
0.015625	0.015625	0.224E-04	0.841E-04	0.107E-02	0.712E-04
0.000390625	0.000390625	0.142E-05	0.522E-05	0.262E-03	0.442E-05

Table 3: test 1 - convergence in maximum norm at the time moment t=0.1

$\triangle x$	$\triangle t$	$\|\epsilon_u\|_c$	$\|\epsilon_p\|_c$	$\|\epsilon_v\|_c$	$\|\epsilon_s\|_c$
0.1	0.1	0.645E-01	0.963E-01	0.145E+00	0.581E-01
0.025	0.025	0.620E-02	0.481E-02	0.619E-02	0.277E-02
0.00625	0.00625	0.382E-03	0.284E-03	0.387E-03	0.151E-03
0.015625	0.015625	0.238E-04	0.174E-04	0.832E-04	0.913E-05
0.000390625	0.000390625	0.148E-05	0.108E-05	0.210E-04	0.566E-06

Table 4: test 1 - convergence in maximum norm at the last time moment t=1

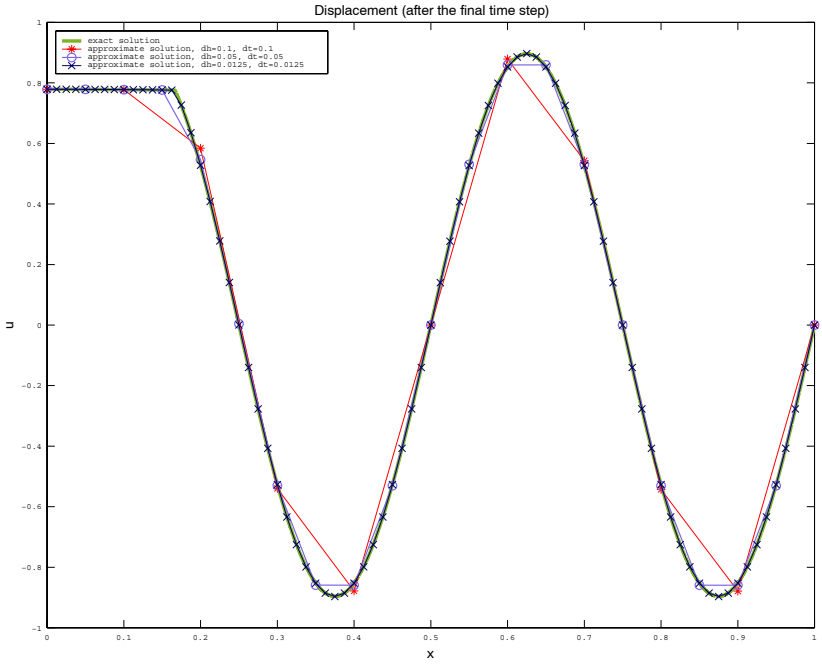

Figure 1: test 1 - convergence of displacements

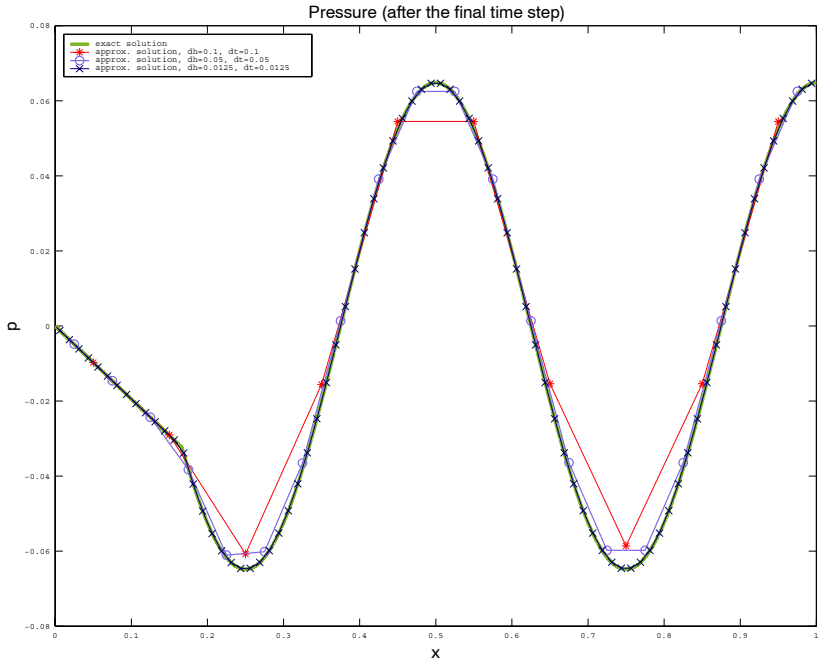

Figure 2: test 1 - convergence of pressure

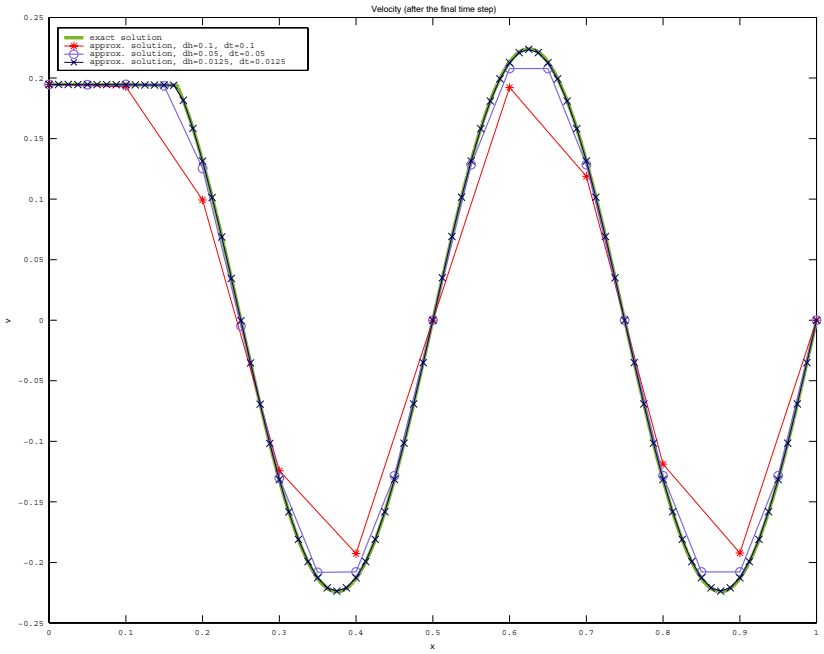

Figure 3: test 1 - convergence of velocity

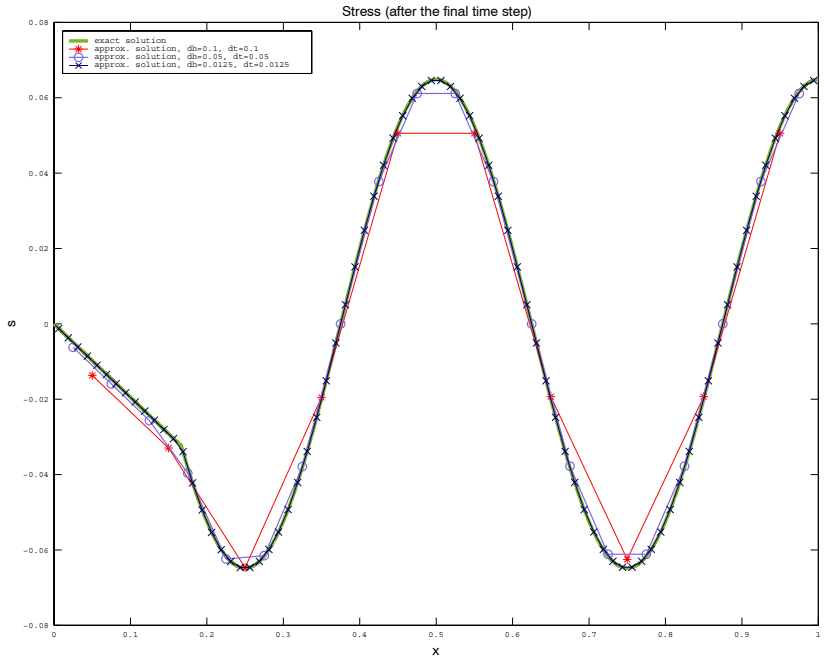

Figure 4: test 1 - convergence of stresses

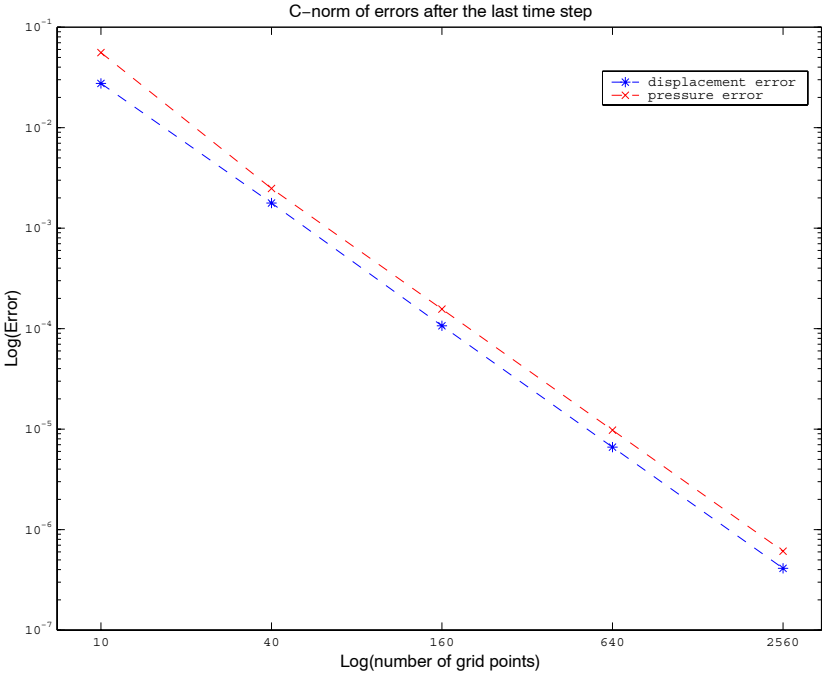

Figure 5: test 1 - pressure and displacement errors

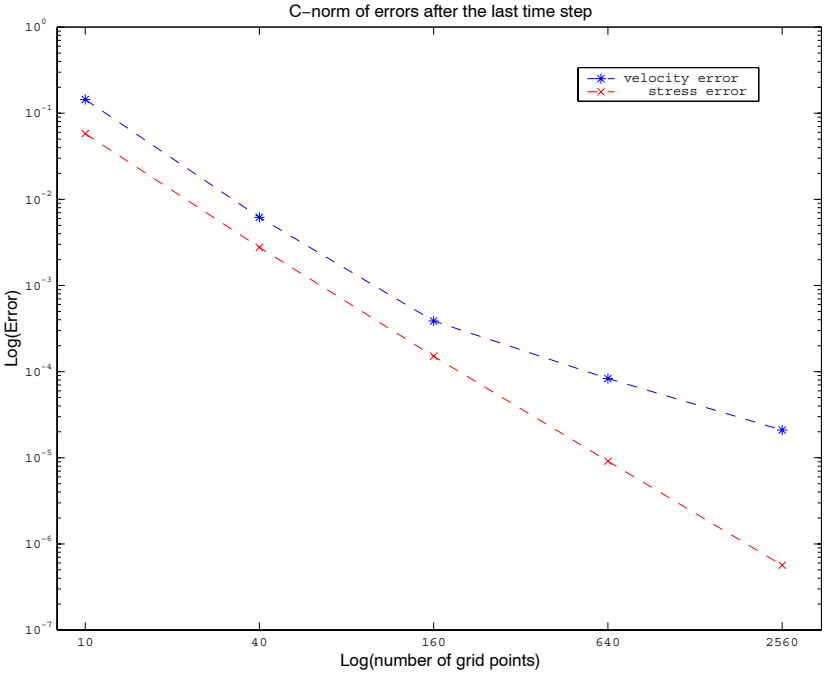

Figure 6: test 1 - velocity and stress errors

Convergence results are summarized in Tables 1 - 4. Note, that values of the grid steps are decreased in a way, preserving a constant value for the parameter θ in the expression $\xi = x_{n-0.5} + \theta h$.
¿From numerical experiments we conclude that displacement and pressure converge with second order in time and space both in L_2 and in maximum norms. We also observe second order of convergence for the stress and first order convergence for the fluid velocity. Fig.5 and Fig.6 illustrate these convergence orders. Fig.1 - Fig.4 represent the analytical solution and numerical solutions calculated on different grids.

Example 2. Input data for the second test are as follows:
$\nu_1 = 1$, $\nu_2 = \frac{\tan(\frac{2}{3})\tan(\frac{23}{3})}{23} \approx 0.1805$, $k_1 = 1$, $k_2 = \frac{1}{23\tan(\frac{2}{3})\tan(\frac{23}{3})} \approx 0.0105$, $a_1 = 0$, $a_2 = 0$, $f(x,t) = 0$. Position of the interface is $\xi = \frac{2}{3}$.
The exact solution is given by

$$p(x,t) = \begin{cases} \cos(\frac{23}{3})\sin(x)e^{-t}, & x \le \frac{2}{3}, \\ \sin(\frac{2}{3})\cos(23(1-x))e^{-t}, & x > \frac{2}{3}, \end{cases}$$

$$u(x,t) = \begin{cases} -\cos(\frac{23}{3})\cos(x)e^{-t}, & x \le \frac{2}{3}, \\ -\frac{1}{23\tan(\frac{2}{3})\tan(\frac{23}{3})}\sin(\frac{2}{3})\sin(23(1-x))e^{-t}, & x > \frac{2}{3}. \end{cases}$$

$$v(x,t) = \begin{cases} \cos(\frac{23}{3})\cos(x)e^{-t}, & x \le \frac{2}{3}, \\ \frac{1}{23\tan(\frac{2}{3})\tan(\frac{23}{3})}\sin(\frac{2}{3})\sin(23(1-x))e^{-t}, & x > \frac{2}{3}, \end{cases}$$

$$s(x,t) = \begin{cases} \cos(\frac{23}{3})\sin(x)e^{-t}, & x \le \frac{2}{3}, \\ \sin(\frac{2}{3})\cos(23(1-x))e^{-t}, & x > \frac{2}{3}. \end{cases}$$

Example 2 is similar to example 1, but with different ratios of the discontinuous coefficients. Convergence results for example 2 are summarized in Table 5 - Table 8. The convergence order for all the variables is the same as in example 1, as it can be also seen from Fig. 11 and Fig. 12. Figures 7 - 10 represent the analytical and the numerical solutions. Note that compared to example 1, coarse grid solutions in this example are less accurate.

$\triangle x$	$\triangle t$	$\|\epsilon_u\|_c$	$\|\epsilon_p\|_c$	$\|\epsilon_v\|_c$	$\|\epsilon_s\|_c$
0.1	0.1	0.341E+00	0.221E+00	0.391E+00	0.187E+00
0.025	0.025	0.270E-01	0.217E-01	0.532E-01	0.167E-01
0.00625	0.00625	0.159E-02	0.132E-02	0.119E-01	0.103E-02
0.015625	0.015625	0.977E-04	0.811E-04	0.291E-02	0.637E-04
0.000390625	0.000390625	0.608E-05	0.504E-05	0.723E-03	0.397E-05

Table 5: test 2 - convergence in maximum norm at the time moment t=0.1

$\triangle x$	$\triangle t$	$\|\epsilon_u\|_c$	$\|\epsilon_p\|_c$	$\|\epsilon_v\|_c$	$\|\epsilon_s\|_c$
0.1	0.1	0.341E+00	0.221E+00	0.391E+00	0.187E+00
0.025	0.025	0.270E-01	0.217E-01	0.532E-01	0.167E-01
0.00625	0.00625	0.159E-02	0.132E-02	0.119E-01	0.103E-02
0.015625	0.015625	0.977E-04	0.811E-04	0.291E-02	0.637E-04
0.000390625	0.000390625	0.608E-05	0.504E-05	0.723E-03	0.397E-05

Table 6: test 2 - convergence in maximum norm at the last time moment t=1

$\triangle x$	$\triangle t$	$\|\epsilon_u\|_{L_2}$	$\|\epsilon_p\|_{L_2}$	$\|\epsilon_v\|_{l_2}$	$\|\epsilon_s\|_{L_2}$
0.1	0.1	0.335E-01	0.903E-01	0.642E+00	0.940E-01
0.025	0.025	0.435E-02	0.516E-02	0.579E-01	0.565E-02
0.00625	0.00625	0.263E-03	0.321E-03	0.633E-02	0.341E-03
0.015625	0.015625	0.164E-04	0.201E-04	0.768E-03	0.212E-04
0.000390625	0.000390625	0.251E-05	0.172E-05	0.194E-04	0.174E-05

Table 7: test 2 - convergence in L_2 norm at the time moment t=0.1

$\triangle x$	$\triangle t$	$\|\epsilon_u\|_{L_2}$	$\|\epsilon_p\|_{L_2}$	$\|\epsilon_v\|_{l_2}$	$\|\epsilon_s\|_{L_2}$
0.1	0.1	0.176E+00	0.816E-01	0.148E+00	0.815E-01
0.025	0.025	0.109E-01	0.744E-02	0.108E-01	0.752E-02
0.00625	0.00625	0.653E-03	0.448E-03	0.126E-02	0.454E-03
0.015625	0.015625	0.403E-04	0.276E-04	0.156E-03	0.280E-04
0.000390625	0.000390625	0.251E-05	0.172E-05	0.194E-04	0.174E-05

Table 8: test 2 - convergence in L_2 norm at the last time moment t=1

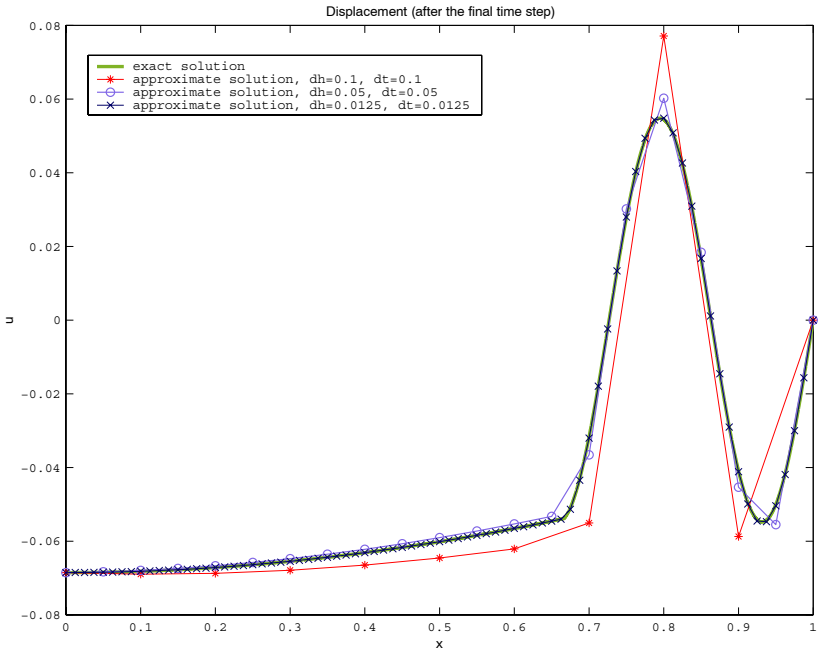

Figure 7: test 2 - convergence of displacement

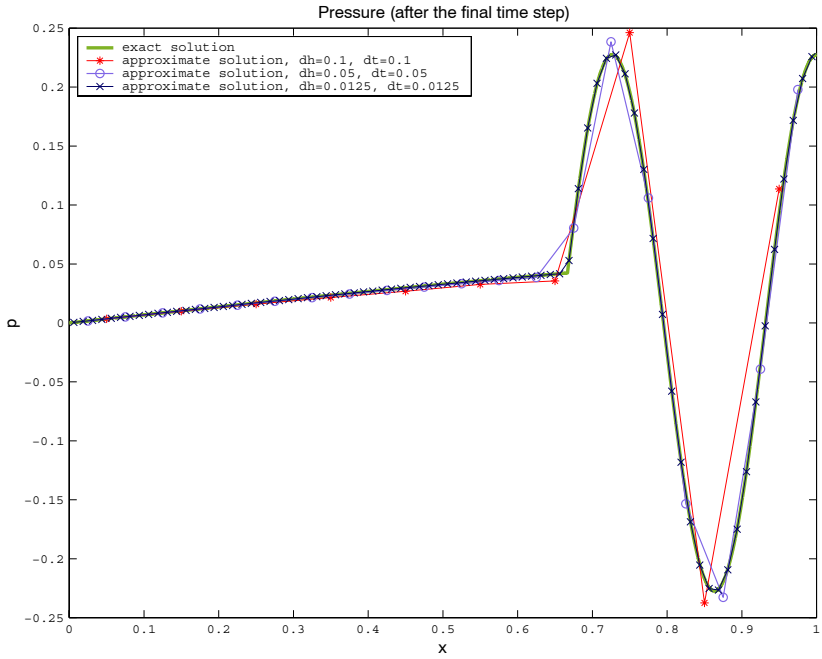

Figure 8: test 2 - convergence of pressure

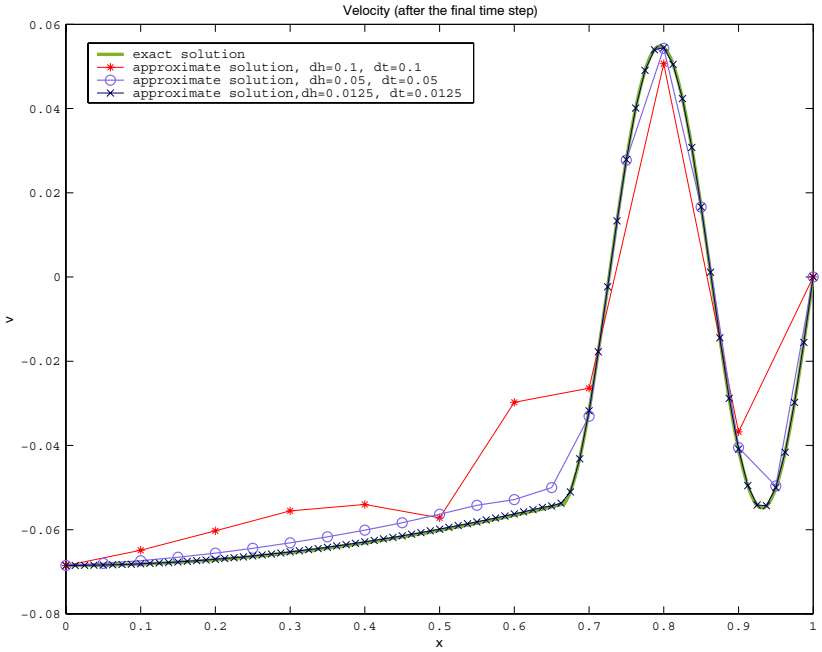

Figure 9: test 2 - convergence of velocity

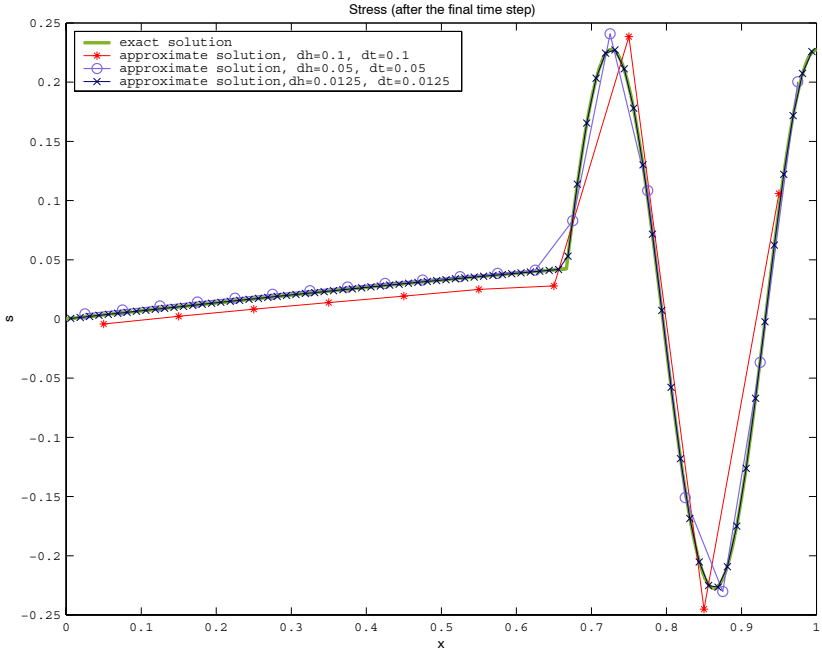

Figure 10: test 2 - convergence of stress

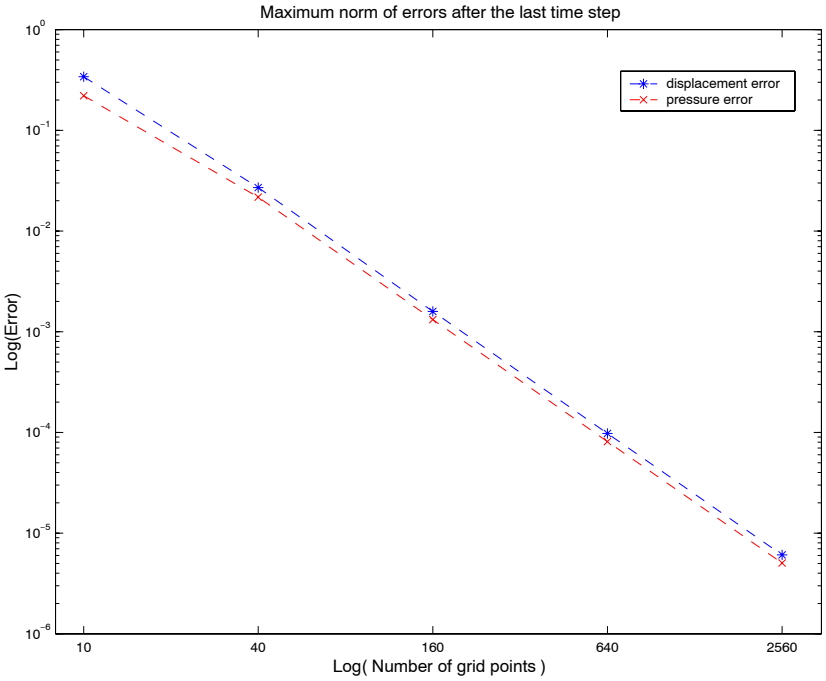

Figure 11: test 2 - pressure and displacement errors

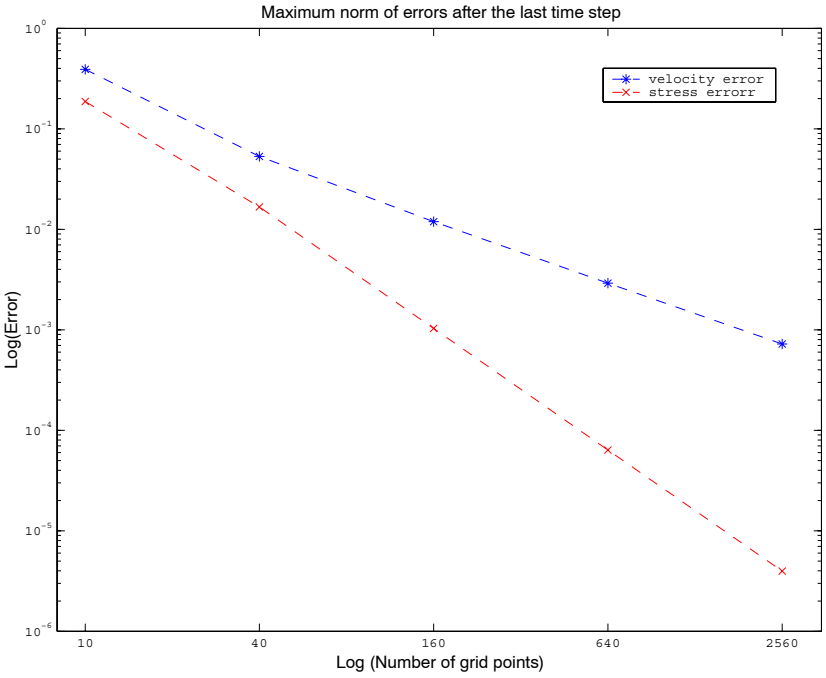

Figure 12: test 2 - velocity and stress errors

$\triangle x$	$\triangle t$	$\|\epsilon_u\|_c$	$\|\epsilon_p\|_c$	$\|\epsilon_v\|_c$	$\|\epsilon_s\|_c$
0.1	0.1	0.542E-02	0.270E-01	0.696E-01	0.308E-01
0.025	0.025	0.116E-02	0.210E-02	0.468E-02	0.209E-02
0.00625	0.00625	0.730E-04	0.151E-03	0.581E-03	0.139E-03
0.015625	0.015625	0.453E-05	0.963E-05	0.132E-03	0.907E-05
0.000390625	0.000390625	0.282E-06	0.608E-06	0.322E-04	0.575E-06

Table 9: test 3 - convergence in maximum norm at the time level t=0.1

Example 3. In the third test we consider compressible fluid (a_1 and a_2 are nonzero). The following values for the coefficients are used:
$\nu_1 = 1$, $\nu_2 = \frac{\tan(\frac{2}{3})\tan(\frac{10}{3})}{10} \approx 0.0153$, $k_1 = 1$, $k_2 = \frac{1}{10\tan(\frac{2}{3})\tan(\frac{10}{3})} \approx 0.6547$, $a_1 = 0.01$, $a_2 = \frac{10.1}{\tan(\frac{2}{3})\tan(\frac{10}{3})} \approx 0.6547$, $f(x,t) = 0$. Position of the interface is $\xi = \frac{2}{3}$. Exact solution is

$$p(x,t) = \begin{cases} \cos(\frac{10}{3})\sin(x)e^{-\frac{100}{101}t}, & x \le \frac{2}{3}, \\ \sin(\frac{2}{3})\cos(10(1-x))e^{-\frac{100}{101}t}, & x > \frac{2}{3}, \end{cases}$$

$$u(x,t) = \begin{cases} -\cos(\frac{10}{3})\cos(x)e^{-\frac{100}{101}t}, & x \le \frac{2}{3}, \\ -\frac{1}{10\tan(\frac{2}{3})\tan(\frac{10}{3})}\sin(\frac{2}{3})\sin(10(1-x))e^{-\frac{100}{101}t}, & x > \frac{2}{3}. \end{cases}$$

$$v(x,t) = \begin{cases} \cos(\frac{10}{3})\cos(x)e^{-\frac{100}{101}t}, & x \le \frac{2}{3}, \\ \frac{1}{10\tan(\frac{2}{3})\tan(\frac{10}{3})}\sin(\frac{2}{3})\sin(10(1-x))e^{-\frac{100}{101}t}, & x > \frac{2}{3}, \end{cases}$$

$$s(x,t) = \begin{cases} \cos(\frac{10}{3})\sin(x)e^{-\frac{100}{101}t}, & x \le \frac{2}{3}, \\ \sin(\frac{2}{3})\cos(10(1-x))e^{-\frac{100}{101}t}, & x > \frac{2}{3}. \end{cases}$$

Convergence results for example 3 are summarized in the Tables 9 - 12. The convergence orders for the compressible case are the same as for the incompressible as it is illustrated in Fig.17 and Fig.18. Analytical and numerical solutions are plotted on Fig.13 - Fig.16.

$\triangle x$	$\triangle t$	$\|\epsilon_u\|_c$	$\|\epsilon_p\|_c$	$\|\epsilon_v\|_c$	$\|\epsilon_s\|_c$
0.1	0.1	0.631E-01	0.621E-01	0.301E-01	0.422E-01
0.025	0.025	0.471E-02	0.423E-02	0.183E-02	0.231E-02
0.00625	0.00625	0.300E-03	0.265E-03	0.107E-03	0.149E-03
0.015625	0.015625	0.188E-04	0.165E-04	0.206E-04	0.937E-05
0.000390625	0.000390625	0.118E-05	0.103E-05	0.477E-05	0.586E-06

Table 10: test 3 - convergence in maximum norm at the last time level t=1

$\triangle x$	$\triangle t$	$\|\epsilon_u\|_{L_2}$	$\|\epsilon_p\|_{L_2}$	$\|\epsilon_v\|_{l_2}$	$\|\epsilon_s\|_{L_2}$
0.1	0.1	0.289E-02	0.128E-01	0.358E-01	0.139E-01
0.025	0.025	0.275E-03	0.938E-03	0.194E-02	0.861E-03
0.00625	0.00625	0.163E-04	0.689E-04	0.125E-03	0.641E-04
0.015625	0.015625	0.101E-05	0.443E-05	0.931E-05	0.419E-05
0.000390625	0.000390625	0.627E-07	0.279E-06	0.859E-06	0.264E-06

Table 11: test 3 - convergence in L_2 norm at the time level t=0.1

$\triangle x$	$\triangle t$	$\|\epsilon_u\|_{L_2}$	$\|\epsilon_p\|_{L_2}$	$\|\epsilon_v\|_{l_2}$	$\|\epsilon_s\|_{L_2}$
0.1	0.1	0.277E-01	0.219E-01	0.967E-02	0.206E-01
0.025	0.025	0.183E-02	0.169E-02	0.530E-03	0.152E-02
0.00625	0.00625	0.117E-03	0.108E-03	0.324E-04	0.974E-04
0.015625	0.015625	0.733E-05	0.681E-05	0.217E-05	0.613E-05
0.000390625	0.000390625	0.459E-06	0.426E-06	0.171E-06	0.384E-06

Table 12: test 3 - convergence in L_2 norm at the last time level t=1

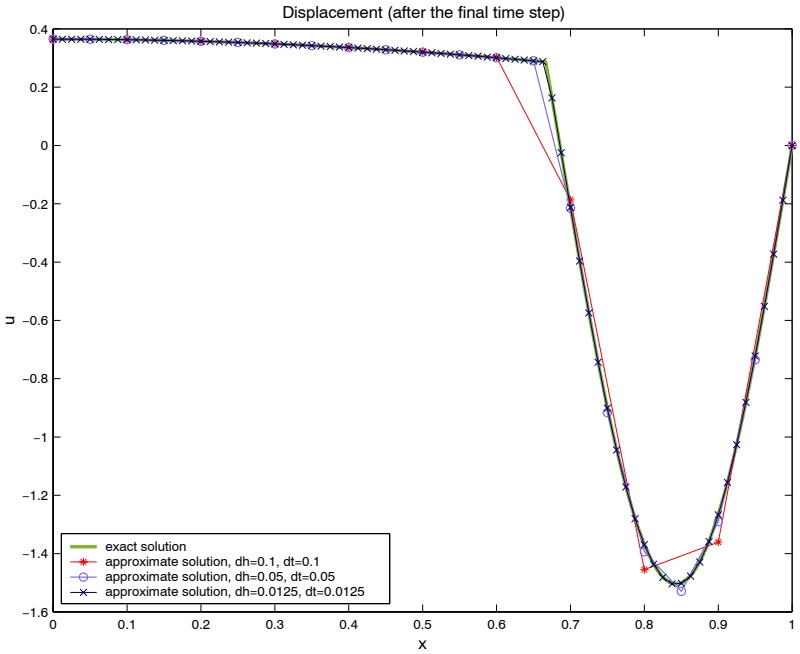

Figure 13: test 3 - convergence of displacement

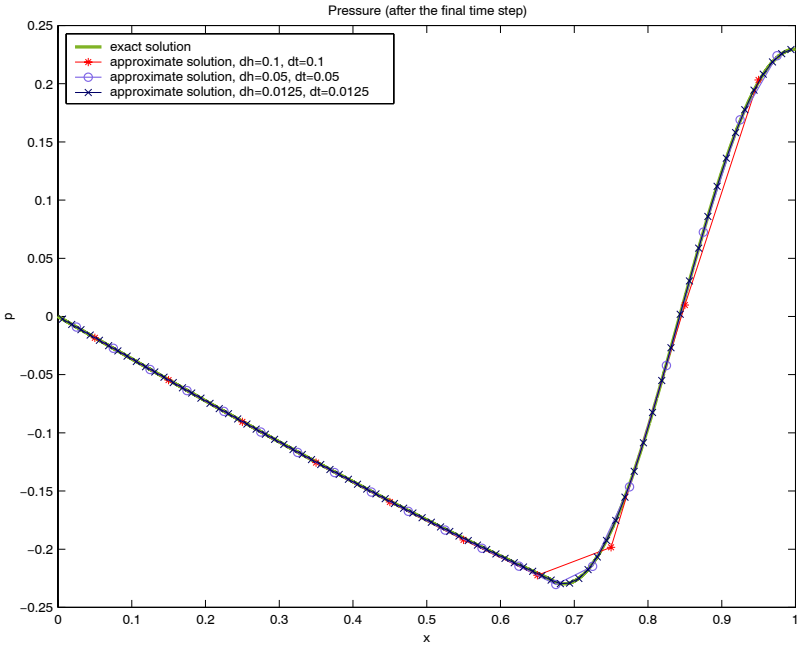

Figure 14: test 3 - convergence of pressure

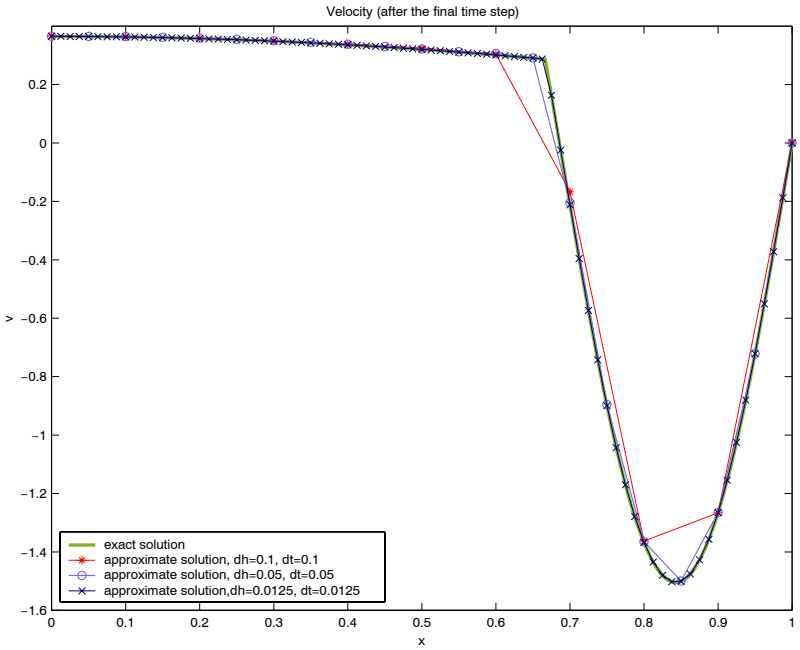

Figure 15: test 3 - convergence of velocity

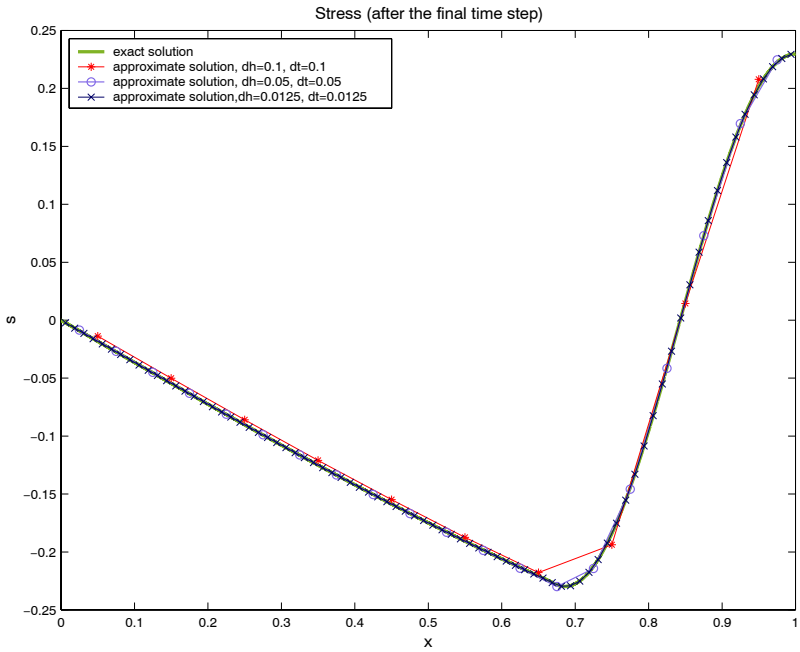

Figure 16: test 3 - convergence of stress

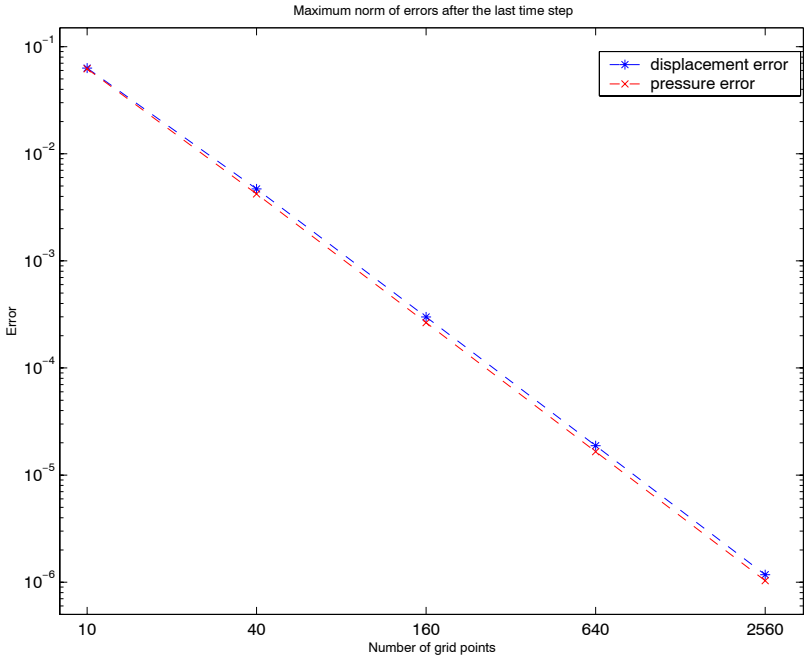

Figure 17: test 3 - pressure and displacement errors

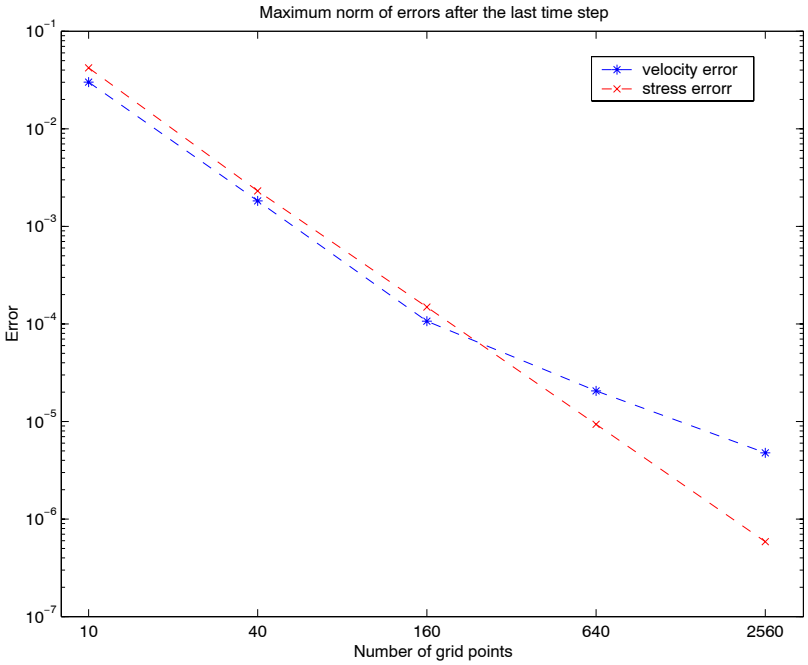

Figure 18: test 3 - velocity and stress errors

$\triangle x$	$\triangle t$	$\|\epsilon_u\|_c$	$\|\epsilon_p\|_c$	$\|\epsilon_v\|_c$	$\|\epsilon_s\|_c$
0.1	0.1	0.632E+00	0.105E+01	0.197E+02	0.101E+01
0.025	0.025	0.151E+00	0.157E+00	0.549E+01	0.142E+00
0.00625	0.00625	0.991E-02	0.102E-01	0.134E+01	0.909E-02
0.015625	0.015625	0.617E-03	0.641E-03	0.326E+00	0.568E-03
0.000390625	0.000390625	0.388E-04	0.400E-04	0.808E-01	0.355E-04

Table 13: test 4 - convergence in maximum norm at the time layer t=0.1

Example 4. In the fourth test we consider again incompressible fluid, but the ratio between coefficients k_1 and k_2 is large (about four orders of magnitude). The values for the coefficients are the following:
$\nu_1 = 1$, $\nu_2 = \frac{1}{100}\tan(\frac{8}{15})\tan(\frac{80}{3}) \approx 0.1601$, $k_1 = 1$, $k_2 = \frac{1}{\tan(100\frac{8}{15})\tan(\frac{80}{3})} \approx 6.2479 \cdot 10^{-4}$, $a_1 = 0$, $a_2 = 0$, $f(x,t) = 0$. Position of the interface is $\xi = \frac{2}{3}$. The exact solution of the problem (6) (with another initial conditions) is given by

$$p(x,t) = \begin{cases} \cos(\frac{10}{3})\sin(\frac{4}{5}x)e^{-\frac{16}{25}t}, & x \le \frac{2}{3}, \\ \sin(\frac{8}{15})\cos(80(1-x))e^{-\frac{16}{25}t}, & x > \frac{2}{3}, \end{cases}$$

$$u(x,t) = \begin{cases} -\frac{5}{4}\cos(\frac{10}{3})\cos(\frac{4}{5}x)e^{-\frac{16}{25}t}, & x \le \frac{2}{3}, \\ -\frac{5\cos(\frac{8}{15})}{4\tan(\frac{80}{3})}\sin(80(1-x))e^{-\frac{16}{25}t}, & x > \frac{2}{3}. \end{cases}$$

$$v(x,t) = \begin{cases} \cos(\frac{10}{3})\cos(\frac{4}{5}x)e^{-\frac{16}{25}t}, & x \le \frac{2}{3}, \\ \frac{\cos\frac{8}{15}}{100\tan(\frac{80}{3})}\sin(80(1-x))e^{-\frac{16}{25}t}, & x > \frac{2}{3}, \end{cases}$$

$$s(x,t) = \begin{cases} \cos(\frac{10}{3})\sin(\frac{4}{5}x)e^{-\frac{16}{25}t}, & x \le \frac{2}{3}, \\ \sin(\frac{8}{15})\cos(80(1-x))e^{-\frac{16}{25}t}, & x > \frac{2}{3}. \end{cases}$$

Convergence resultes are summarized in Tables 13 - 16. It is seen that convergence order does not depend on the jumps of coefficients (see also Fig.23 - Fig.24). At the same time, the numerical solution on very coarse grids can

$\triangle x$	$\triangle t$	$\|\epsilon_u\|_c$	$\|\epsilon_p\|_c$	$\|\epsilon_v\|_c$	$\|\epsilon_s\|_c$
0.1	0.1	0.155E+01	0.138E+01	0.189E+01	0.114E+01
0.025	0.025	0.185E+00	0.380E-01	0.867E+00	0.401E-01
0.00625	0.00625	0.138E-01	0.413E-02	0.165E+00	0.401E-02
0.015625	0.015625	0.811E-03	0.226E-03	0.379E-01	0.224E-03
0.000390625	0.000390625	0.496E-04	0.135E-04	0.928E-02	0.136E-04

Table 14: test 4 - convergence in maximum norm at the last time moment t=1

$\triangle x$	$\triangle t$	$\|\epsilon_u\|_{L_2}$	$\|\epsilon_p\|_{L_2}$	$\|\epsilon_v\|_{l_2}$	$\|\epsilon_s\|_{L_2}$
0.1	0.1	0.258E+00	0.455E+00	0.804E+01	0.455E+00
0.025	0.025	0.656E-01	0.602E-01	0.101E+01	0.615E-01
0.00625	0.00625	0.454E-02	0.380E-02	0.115E+00	0.387E-02
0.015625	0.015625	0.285E-03	0.238E-03	0.140E-01	0.242E-03
0.000390625	0.000390625	0.179E-04	0.148E-04	0.174E-02	0.151E-04

Table 15: test 4 - convergence in L_2 norm at the time moment t=0.1

$\triangle x$	$\triangle t$	$\|\epsilon_u\|_{L_2}$	$\|\epsilon_p\|_{L_2}$	$\|\epsilon_v\|_{l_2}$	$\|\epsilon_s\|_{L_2}$
0.1	0.1	0.843E+00	0.542E+00	0.754E+00	0.521E+00
0.025	0.025	0.757E-01	0.823E-02	0.204E+00	0.819E-02
0.00625	0.00625	0.480E-02	0.123E-02	0.186E-01	0.124E-02
0.015625	0.015625	0.296E-03	0.773E-04	0.209E-02	0.774E-04
0.000390625	0.000390625	0.184E-04	0.481E-05	0.254E-03	0.481E-05

Table 16: test 4 - convergence in L_2 norm at the last time moment t=1

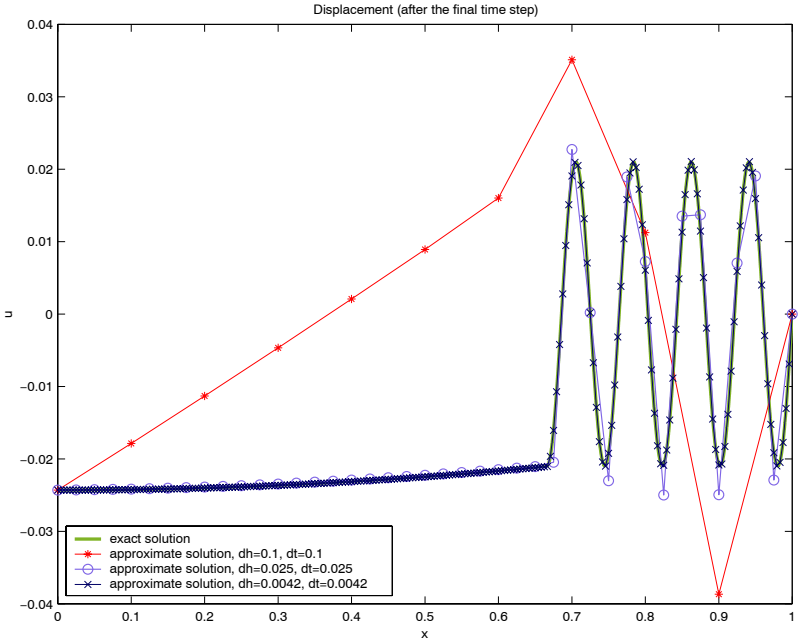

Figure 19: test 4 - convergence of displacement

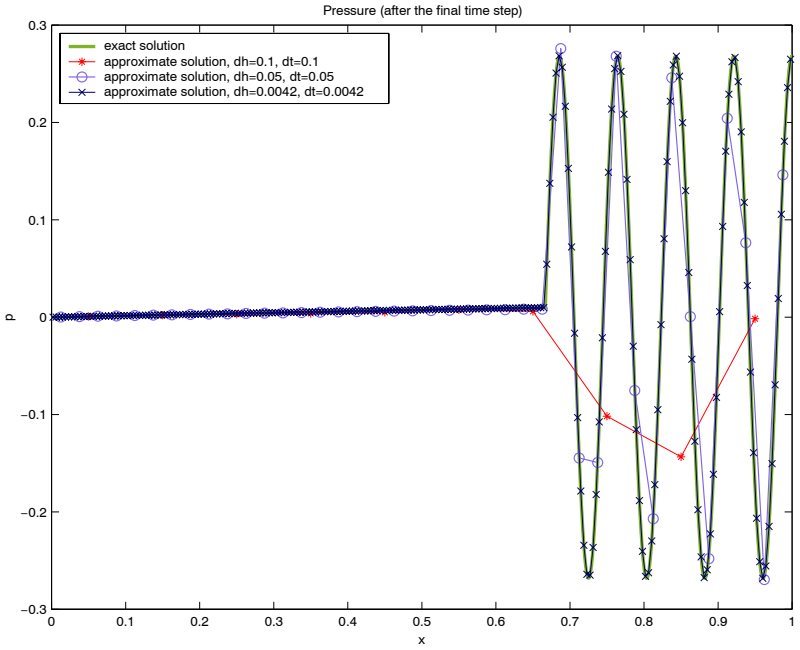

Figure 20: test 4 - convergence of pressure

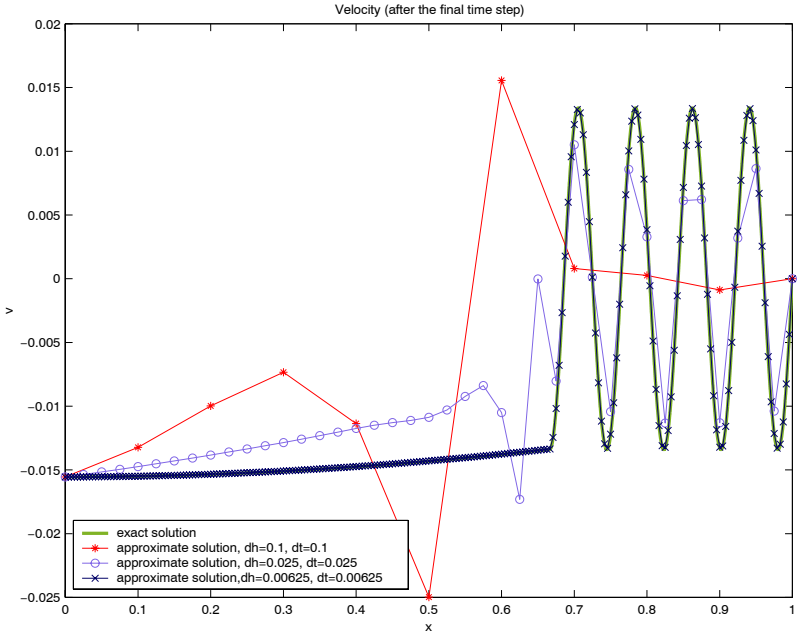

Figure 21: test 4 - convergence of velocity

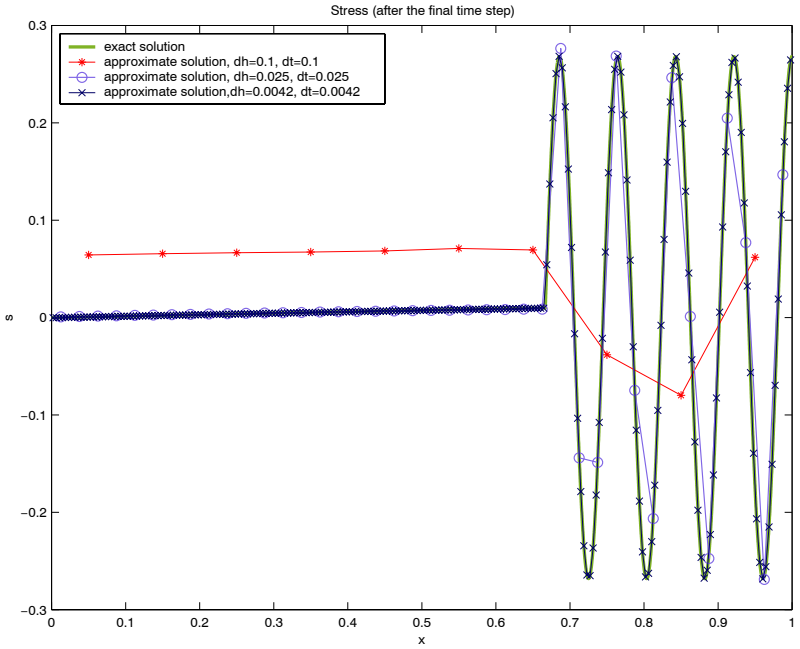

Figure 22: test 4 - convergence of stress

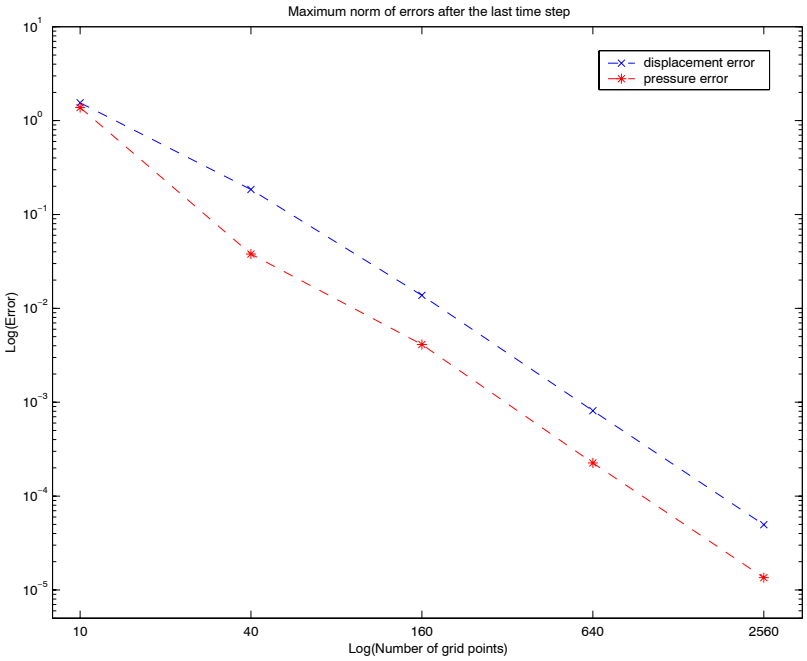

Figure 23: test 4 - pressure and displacement errors

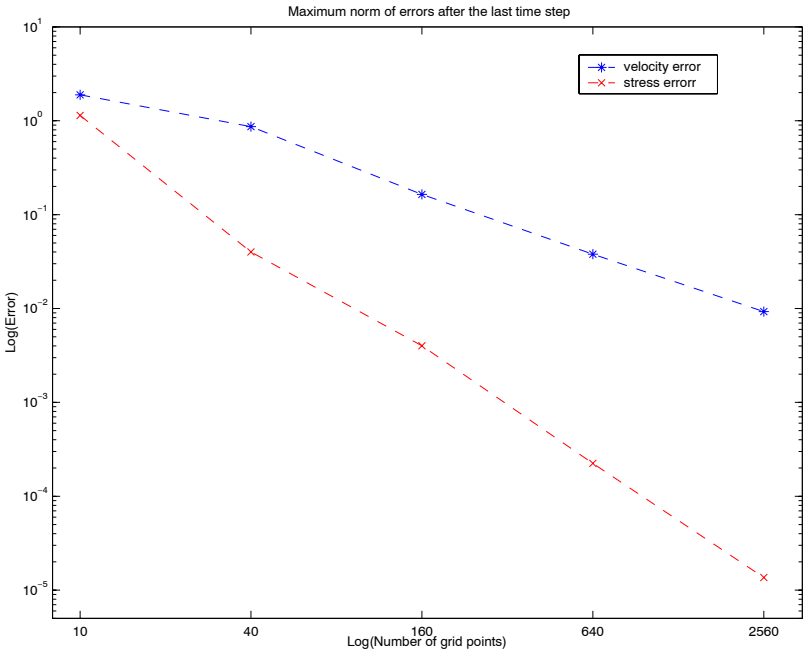

Figure 24: test 4 - velocity and stress errors

give a bad approximation to the exact solution. This can be observed on Fig.19 - Fig.22, where analytical and numerical solutions are plotted.

In the second set of numerical experiments we satisfy all boundary and initial conditions corresponding to the continuous model. Consider the case when pore fluid is incopressible. In such situation initially whole vertical load is taken by the pore fluid and there is a very little compression of the soil sample immediately after placing the load. This means following initial conditions:

$$p(x,0) = \sigma_0,\ u(x,0) = 0.$$

Then during the consolidation process fluid pressure is dissipating and simultaneously effective stress of the solid is increasing. There is no known analytical solution in this case. Note that all paramenters in the tests below are non-dimensional and all results are also plotted non-dimensionally.
Example 5. In this test we consider consolidation of medium consisted of two layers of equal depth. The upper layer is four times more permeable than the lower one and the elasic properties of both layers are identical. This means following values for parameters: $k_1 = 1$, $k_2 = 0.25$, $\nu_1 = 1$, $\nu_2 = 1$. External load is $\sigma_0 = 1$.
Figure 25 shows the degree of consolidation $d(x,t) = 1 - \frac{p(x,t)}{p_0(x,t)}$ inside the soil profile for different time moments; space grid in these calculations consists of 40 nodes. Figure 26 shows consolidation degree at time $t = 0.62$ calculated on grids of different thickness. Results, plotted in Fig. 25 show quite good agreement with results published in the monograph [18], but we suppose that our results are more accurate. (?)
Example 6. In this test material properties of layers are following: $k_1 = 1.0$, $k_2 = 10.0$, $\nu_1 = 1.0$, $\nu_2 = 0.1$. It means that upper layer is ten times less permeable, but ten times stiffer. Figures 27, 28 and 29 show pore pressure, stress of the solid and fluid velocity distributions respectively for the soil profile at different moments of time. Figure 30 shows rate of surface settlement in time. Remind that in this set of numerical experiments exact solution of the problem is unknown and we can not comare it to our numerical results, we can only analyse behaviour of the numerical solution during the grid thickening. Figures 31 - 35 show all quantities of the process calculated on grids of different thickness for a fixed time value $t = 0.05$
Example 7. In this test we change the location of layers from example 6. Now upper layer is ten times more permeable and ten times less stiff. Values of parameters are: $k_1 = 1.0$, $k_2 = 0.1$, $\nu_1 = 1.0$, $\nu_2 = 10.0$. Results for this situation are plotted in figures 36, 37, 38 and 39. Figures 40 - 44 show results calculated on grids of different thickness for a fixed time value $t = 0.05$.

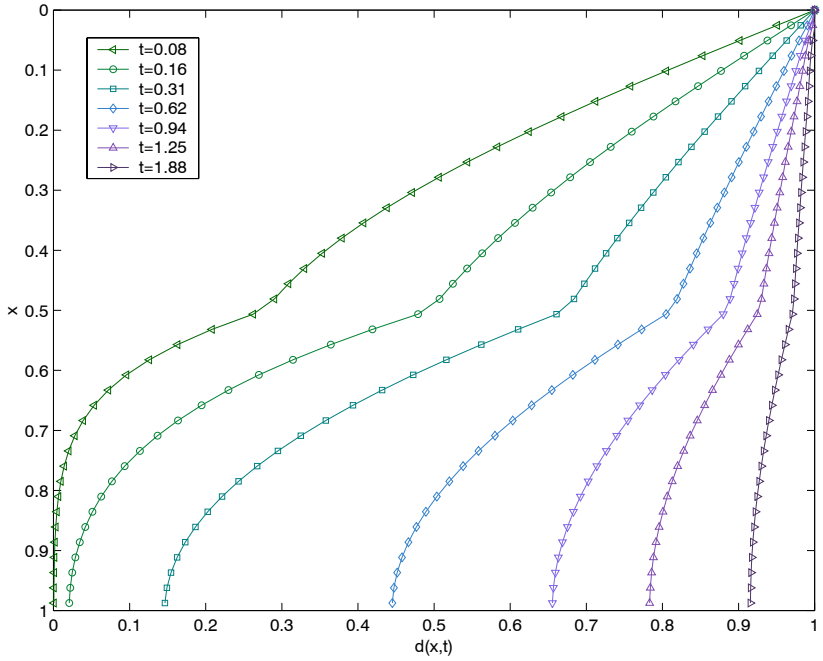

Figure 25: test 5 - degree of consolidation at different moments in time: grid with 40 nodes in space.

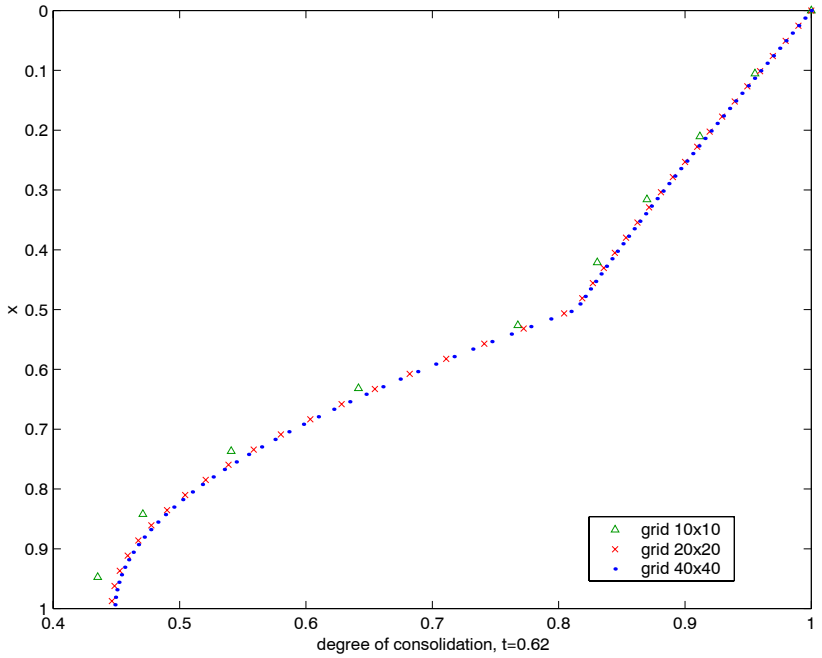

Figure 26: test 5 - degree of consolidation,....

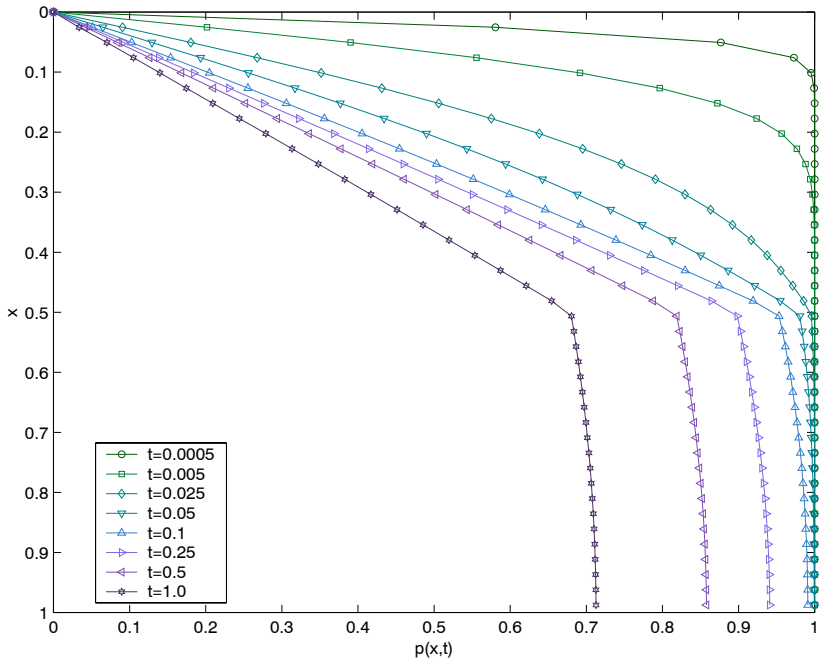

Figure 27: test 6 - pore pressure distribution at different moments in time

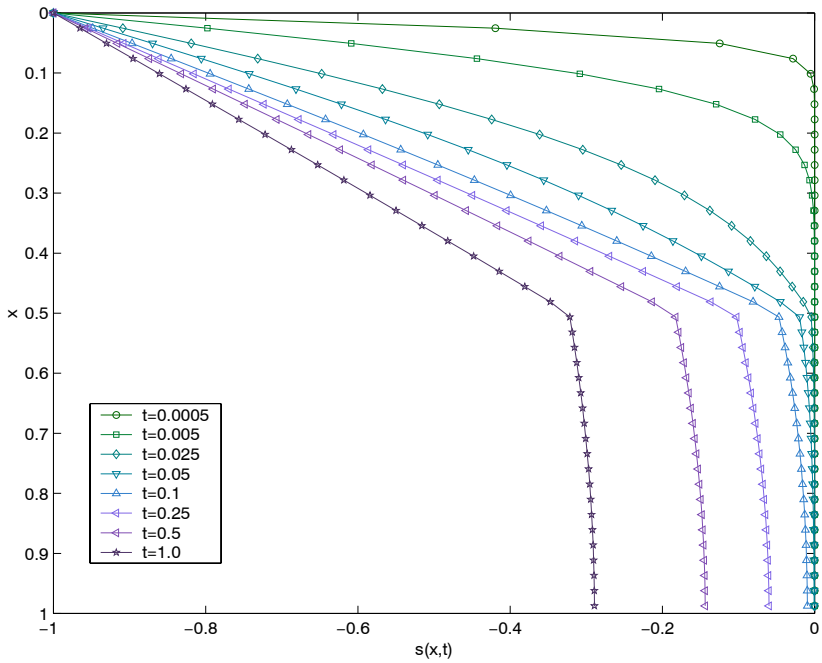

Figure 28: test 6 - stress of the solid at different moments in time

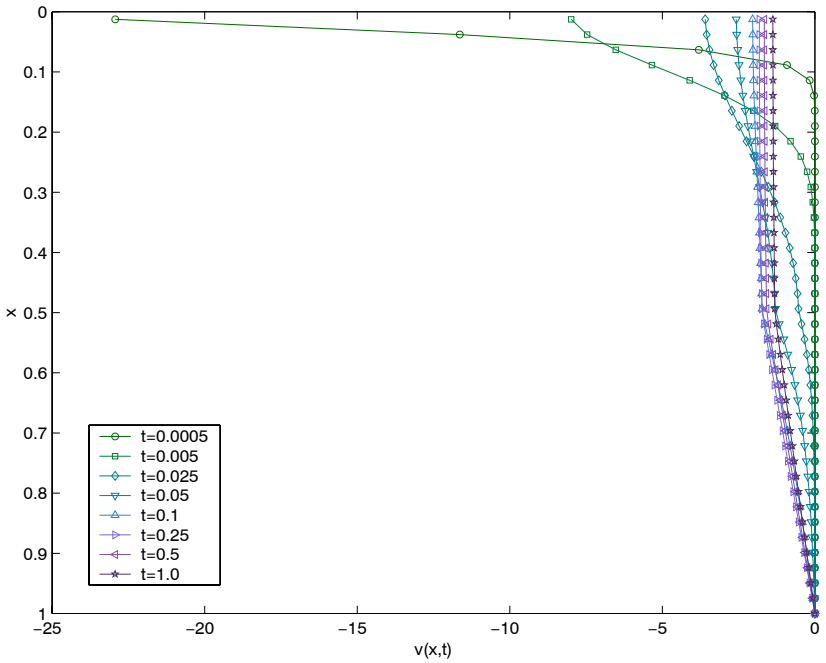

Figure 29: test 6 - fluid velocity at different moments in time

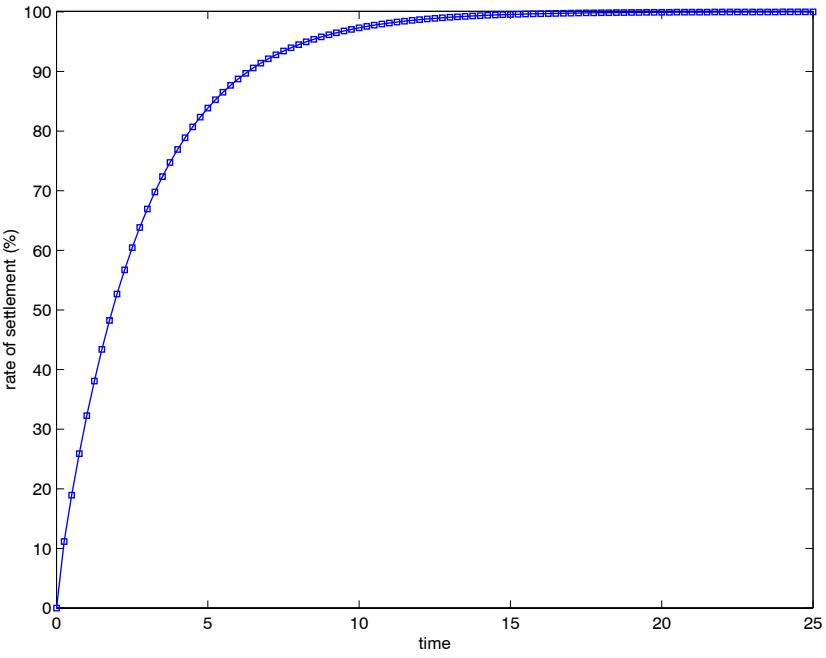

Figure 30: test 6 - rate of settlement of the soil surface

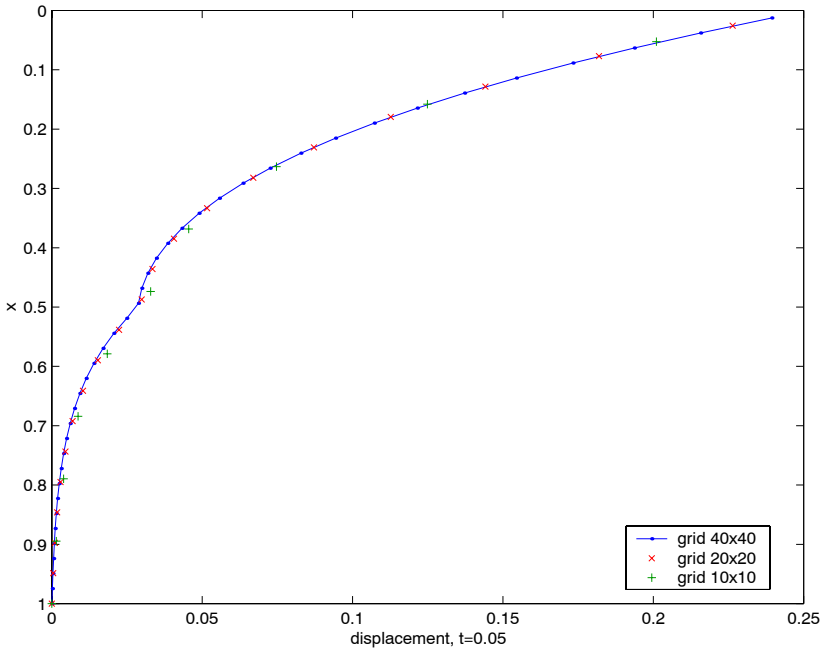

Figure 31: test 6 - displacement of the solid

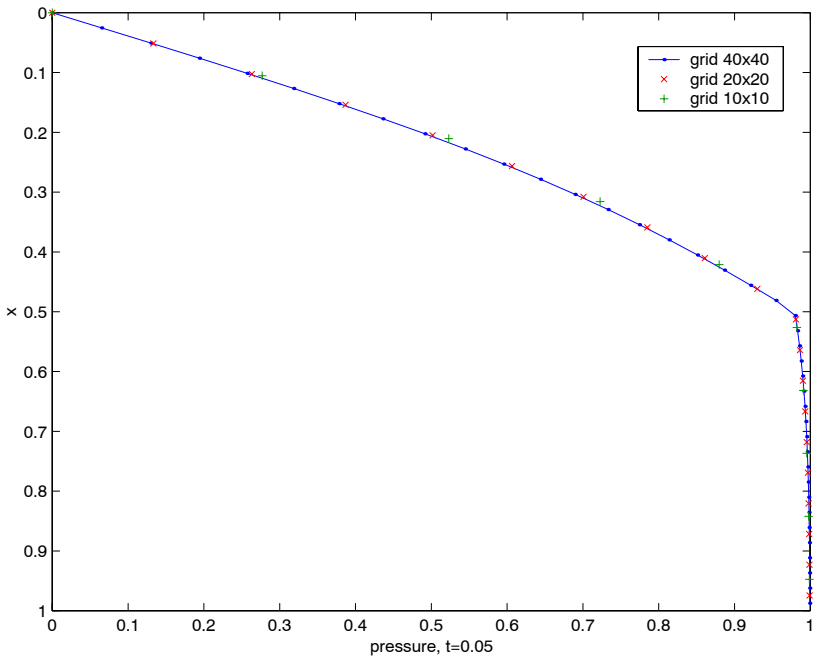

Figure 32: test 6 - pore pressure

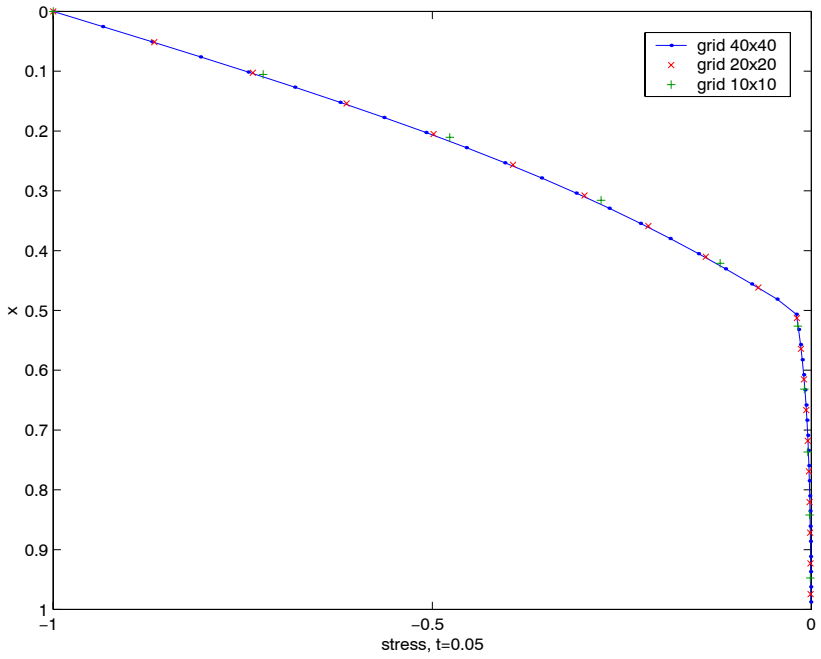

Figure 33: test 6 - stress of the solid

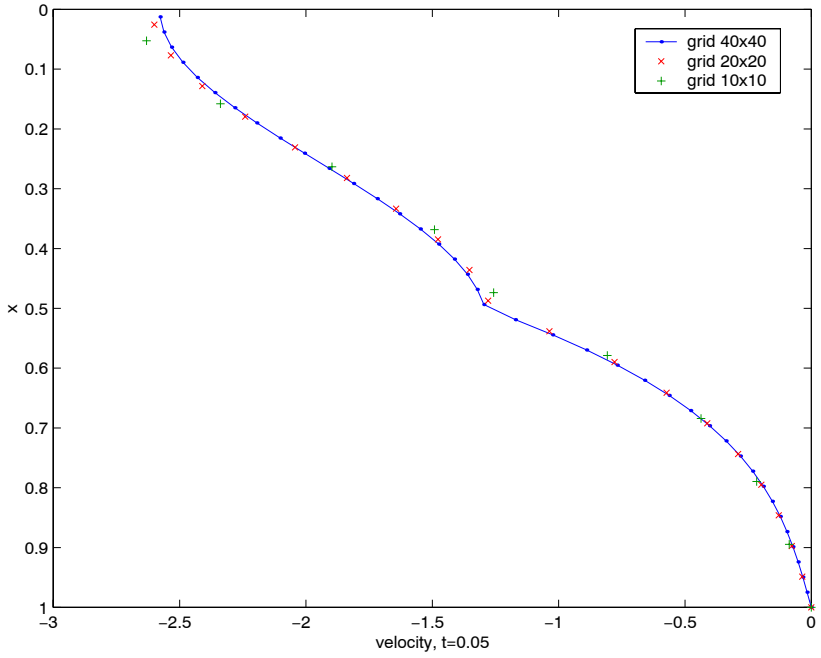

Figure 34: test 6 - fluid velocity

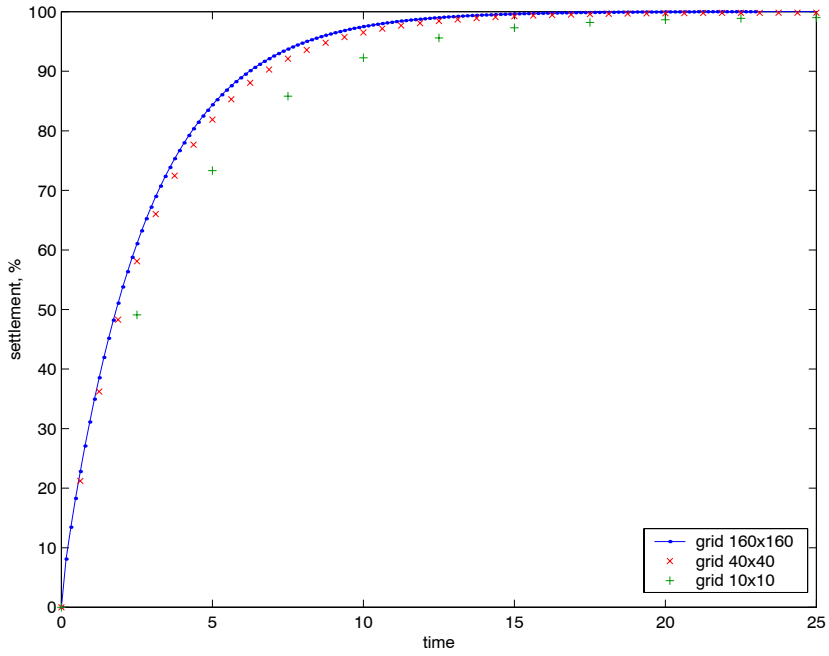

Figure 35: test 6 - rate of settlement of the soil surface

Distributions of pore pressure and rate of settlement obtained in the previous two numerical experiments were compared to results published in the paper [14], and a very good qualitative agreement was observed.

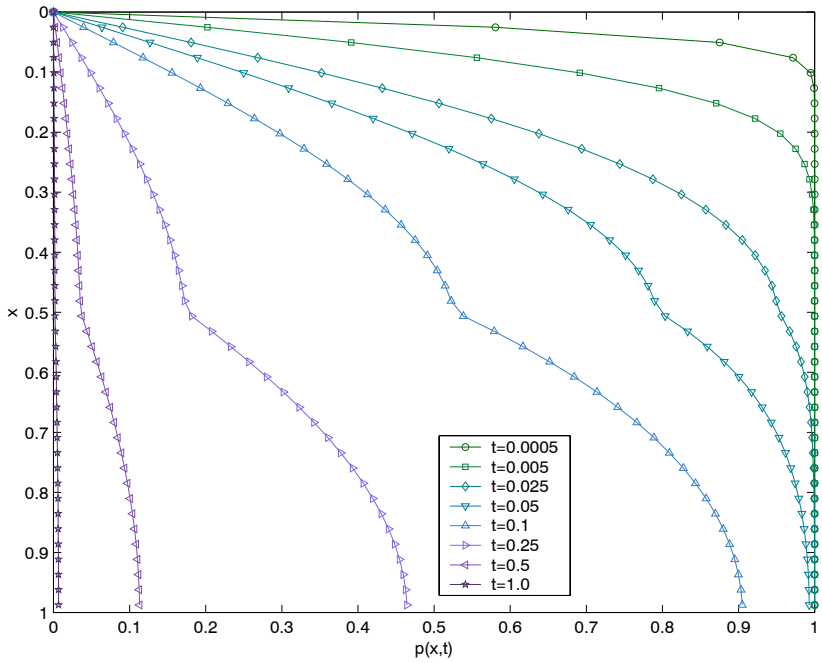

Figure 36: test 7 - pore pressure distribution at different moments in time

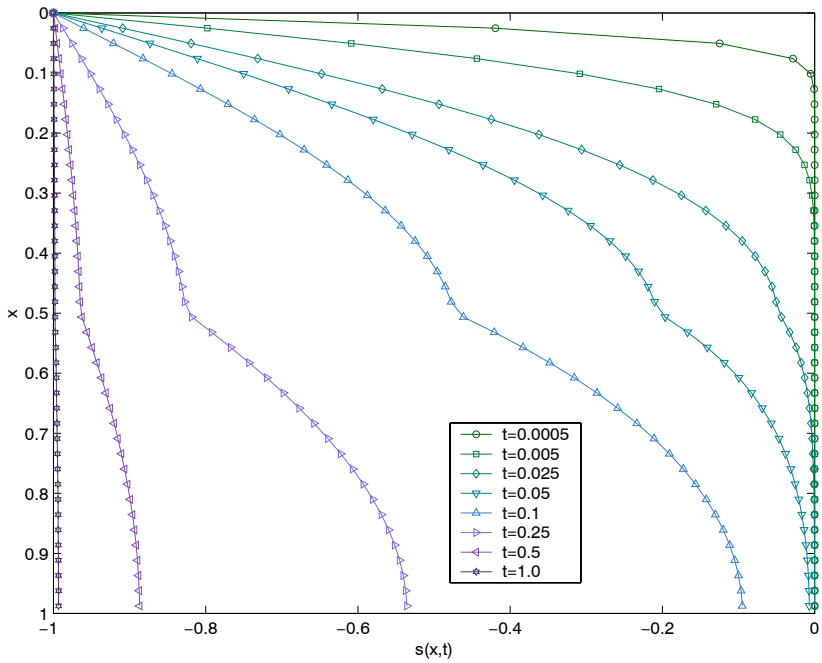

Figure 37: test 7 - stress of the solid at different moments in time

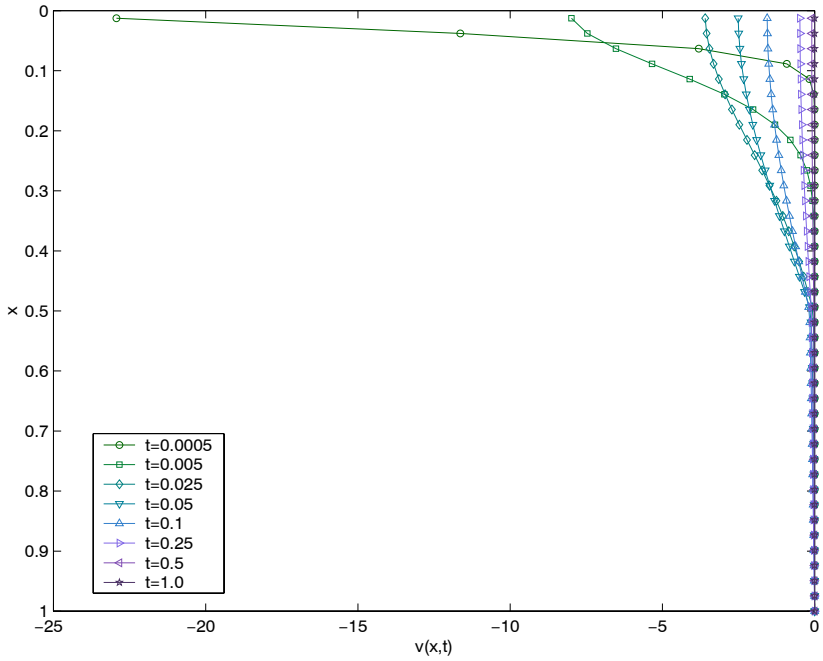

Figure 38: test 7 - fluid velocity at different moments in time

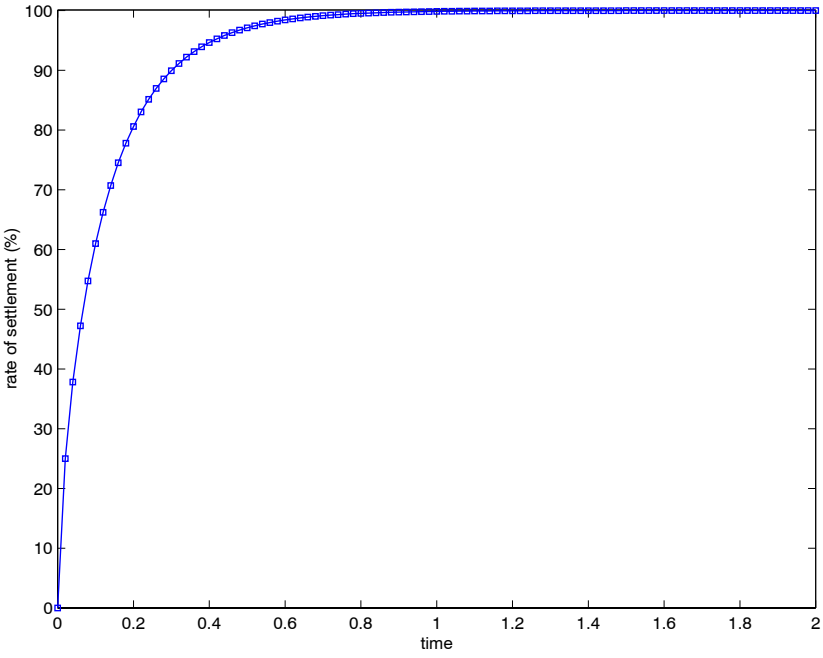

Figure 39: test 7 - rate of settlement of the soil surface

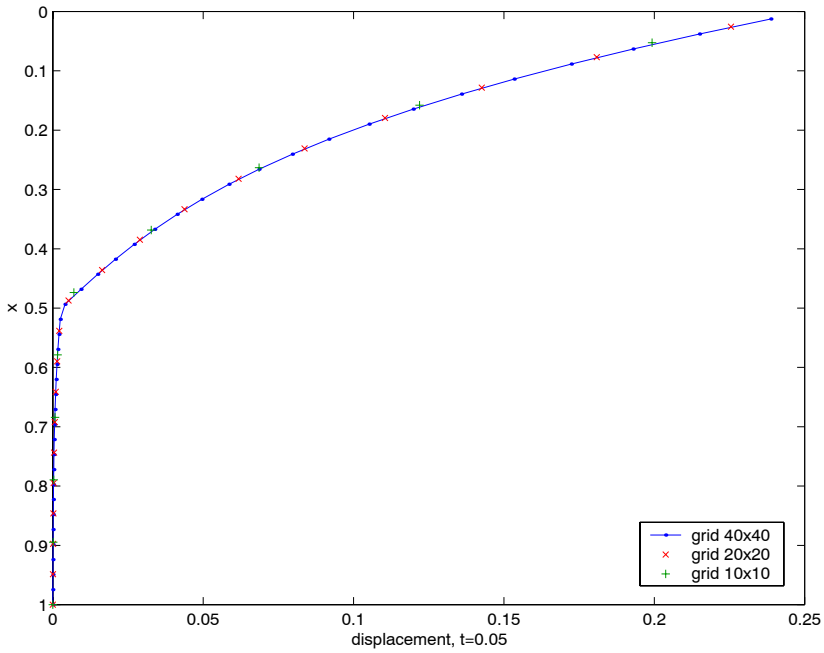

Figure 40: test 7 - displacement of the solid

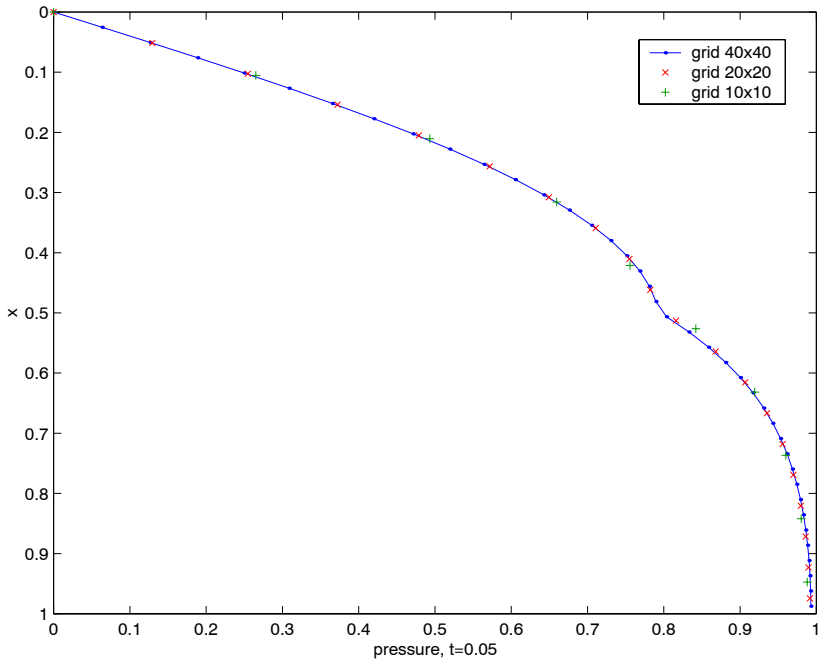

Figure 41: test 7 - pore pressure

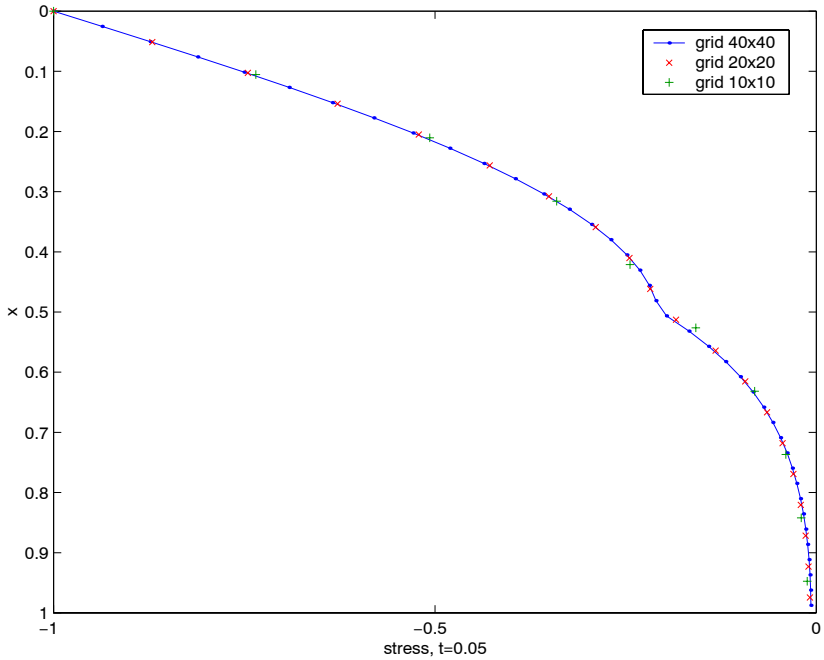

Figure 42: test 7 - stress of the solid

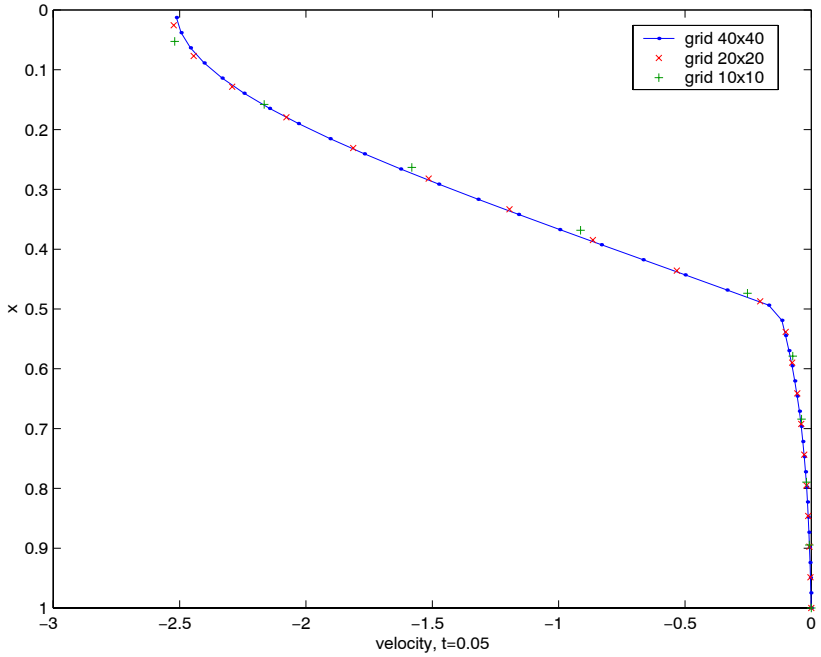

Figure 43: test 7 - fluid velocity

References

[1] M. Biot, General theory of three dimensional consolidation, J. Appl. Phys., 12(1941), pp. 155-169.

[2] J. Bear, Y. Bachmat, Introduction to modelling of transport Phenomena in Porous Media, Kluwer Academic, Dordrecht, 1990.

[3] R.W. Lewis, B.A. Schrefler, The finite element method in the static and dynamic deformation and consolidation of porous media, John Wiley, Chichester, 1998.

[4] F.J. Gaspar, F.J. Lisbona, P.N. Vabischevich, A finite difference analysis of Biot's consolidation model, Appl. Num. Math, 44(2003), pp. 487-506.

[5] F.J. Gaspar, F.J. Lisbona, P.N. Vabischevich, A numerical model for radial flow through porous and deformable shells, CMAM, 4(2004), No.1 , pp. 34-47.

[6] A. A. Samarskii, Theory of difference schemes, Pure and Applied Mathematics, Marcel Dekker, New York, 2001.

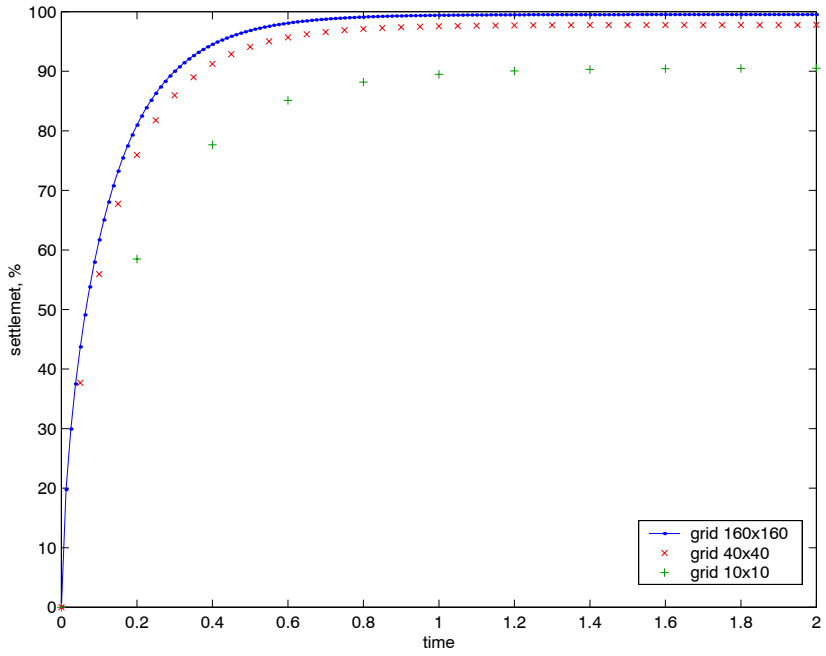

Figure 44: test 7 - rate of settlement of the soil surface

[7] R.E. Showalter, Diffusion in poroelastic media, J. Math. Anal. Appl., 251 (2000), pp. 310-340.

[8] H. F. Wang, Theory of linear poroelasticity with application to geomechanics and hydrogeology, Princeton University Press, Princeton, 2000.

[9] S.I. Barry , G.K. Aldis, Comparison of models for flow induced deformation of soft biological tissue, Australian defence force academy, Canberra, 1996.

[10] L. Li, Theory of poroelastic structures with diffusion in the longitudinal directions, PhD thesis, Ben-Gurion University, Negev, US, 1997.

[11] H. Vomhoff, M. Martinez, B. Norman, The transversal steady-state permeability of a fibre web compressed between rough permeable surfaces, Journal of pulp and paper science, 26(12), 2000, pp. 428-436.

[12] H. Vomhoff, On the in-plane permeability of water-saturated fibre webs, Nordic pulp and paper research journal, 4(15), 2000.

[13] M. Kurashige, H. Takasawa, T. Mori, Ink flow mechanism in a mimeograph machine (Effects of nonlinear elasticity in a porous layer), Nippon Kikai Gakkai Ronbunshu, A Hen/Transactions of the Japan Society of Mechanical Engineers, Part A, v 62, n 594, Feb 1996, JSME, Tokyo, Japan, pp. 533-539.

[14] I.C. Pyrah, One-dimensional consolidation of layered soils, Geotechnique, 46(1996), No.3, pp. 555-560.

[15] M.A. Koenders, R.J. Wakeman, The initial stages of compact formation from suspensions by filtration, Chemical Engineering Science, Vol. 51, No. 16, pp.3897-3908, 1996.

[16] M.A. Koenders, R.J. Wakeman, Filter cake formation from structured suspensions, Trans IChemE, Vol. 75, Part A, March 1997.

[17] M.A. Koenders, S. Reymann, R.J. Wakeman, The intermediate stage of the dead-end filtration process, Chemical Engineering Science 55(2000), pp. 3715-3728.

[18] Braja M. Das, Advanced soil mechanics, First edition, Hemisphere Publ., Washington, 1983.

Acknowledgments. The work has been supported by EC under the project INTAS-30-50-4395.